Climate Dynamics
https://doi.org/10.1007/s00382-018-4569-5

Multidecadal to centennial surface wintertime wind variability over Northeastern North America via statistical downscaling

Etor E. Lucio-Eceiza[1,2,3] · J. Fidel González-Rouco[1,2,3] · Elena García-Bustamante[4] · Jorge Navarro[4] · Hugo Beltrami[5]

Received: 24 April 2018 / Accepted: 3 December 2018

Abstract
The variability of the surface wind field over Northeastern North America was analysed through a statistical downscaling (SD) approach, using the relationships among the main large-scale and observed wind circulation modes. The large-scale variables were provided by 12 global reanalyses. The observed zonal and meridional wind components come from a database of 525 sites spanning over 1953–2010. A large percentage of the regional variability was explained in terms of three major large- and regional/local-scale coupled circulation patterns, accounting for 55.3% (59.3%) of the large (regional/local) scale variability. The method delivered robust results regardless of the SD model configuration, albeit with sensitivity to the number of retained circulation modes and the large-scale window size, but not to the reanalysis chosen for the large-scale variables. The methodological uncertainty was larger for sites/wind components with larger variability. A parameter configuration chosen for yielding the best possible SD estimations showed high correlation values between these estimations and the observations for the majority of the sites (0.6–0.9, significant at $p < 0.05$), and a realistic wind variance (standard deviation ratios between 0.6 and 1.0), with similar results regardless of the reanalysis. The reanalysis direct wind outputs showed higher correlations than the SD estimates (0.7–0.97, also significant). The skill in reproducing observational variance differed considerably from model to model (ratios between 0.5 and 3). The regional wind climatology was reconstructed back to 1850 with the help of century long reanalyses and two additional SLP gridded datasets allowing to estimate the variability at decadal and multidecadal timescales. Recent trends in the wind components are not unusual in the context of century-long reconstructed variability. Extreme values in both components tend to appear associated with high values in the first two modes of variability.

Keywords Surface wind · Statistical downscaling · Spatial and temporal variability · Sensitivity · Reanalysis intercomparison · Past reconstructions · Extreme events

1 Introduction

Surface wind is a fundamental meteorological variable that has an appreciable effect in the society in many day to day applications. Its influence spans over a wide array of topics such as wave formation and ocean mixing (Siegismund and Schrum 2001), pollutant dispersion (Darby 2005), evapotranspiration processes (Farquhar and Roderick 2005), crop growth (Cleugh et al. 1998), and structural vulnerability and insurance losses (Khanduri and Morrow 2003) among many. In addition, the increasing demand of energy has boosted the search for alternative energy forms (e.g., Hughes and Chaudhry 2011; European Horizon 2020 programme). Among them the wind energy has been subject to a fast technological development (e.g. Wiser and Bolinger 2016; REN21 2017). Consequently, works on surface wind

✉ Etor E. Lucio-Eceiza
eelucio@fis.ucm.es

1 Facultad de CC. Físicas, Universidad Complutense Madrid, Madrid, Spain

2 Instituto de Geociencias (UCM-CSIC), Madrid, Spain

3 Dpto. Física de la Tierra y Astrofísica, Fac. CC. Físicas, Universidad Complutense Madrid, Avd. Complutense s/n, 28040 Madrid, Spain

4 División de Energías Renovables, CIEMAT, Madrid, Spain

5 Climate and Atmospheric Sciences Institute, St. Francis Xavier University, Antigonish, NS, Canada

Published online: 11 December 2018

encompass analyses at many different time scales, from its hourly (Tuller 2004; Culver and Monahan 2013) and daily evolution (Martinez et al. 2013; Brinckmann et al. 2016) to its long-term past (Pryor et al. 2009; García-Bustamante et al. 2011) or future (Pryor et al. 2012; Cheng 2014) climatological variability. They also involve the analysis of many different aspects of the wind such as trends (Wan et al. 2010; McVicar et al. 2012), their present (Zha et al. 2017) or future (Pryor et al. 2005) probability distributions, extreme events (Cheng et al. 2014) and wind power assessment (García-Bustamante et al. 2008, 2009) among others.

The surface wind can be seen as the local response to the large scale circulation patterns that is modulated, to a greater o lesser extent, by the orographic, thermal, and geographic characteristics at regional and local scales (e.g., Najac et al. 2009; Wan et al. 2010). Large scale wind data from reanalysis products (e.g., Saha et al. 2010), General Circulation Models (GCM; e.g., Taylor et al. 2012) or observational gridded databases (e.g., Allan and Ansell 2006), otherwise invaluable sources of temporal and spatially continuous climatological information, have, due to their coarse resolution, problems to skilfully address the local variability. Thus, ancillary methodologies are needed to bridge both scales. These, known as *downscaling methodologies* are mainly divided into two approaches. The first approach comprises *Dynamical Downscaling* (DD) techniques and uses Regional Climate Models (RCM, e.g., Pryor et al. 2009; Jiménez et al. 2010) or Numerical Weather Prediction models (NWP, for regional reanalyses, e.g., Mesinger et al. 2006; Bollmeyer et al. 2015) that are usually fed by GCM or reanalysis data. As with the large scale databases, these regional models provide a temporally and spatially continuous set of multiple variables, with horizontal resolutions of up to 2 km (Jiménez et al. 2010). On the downside they are computationally very demanding and usually confined to a limited geographical area and time period. The second approach looks for empirical-statistical relationships among a set of large scale *predictor* variables obtained from either reanalyses, GCMs or observational gridded data, and a local observational *predictand* database (e.g., Zorita and von Storch 1999; Xoplaki et al. 2003). The *statistical downscaling* (SD) techniques offer a computationally relatively inexpensive way of relating these two fields in comparison to DD methodologies, but they are spatially limited to the location of the observational sites. There is a third hybrid approach that combines some aspects of both dynamical and statistical techniques (DSD, e.g., Martinez et al. 2013).

Northeastern North America is a region of high wind speeds all year round (Lucio-Eceiza et al. 2018a, b) as shown by the spatial distribution of mean wind speeds in Fig. 1a. Due to its favourable geographical location, the large-scale dynamics foster the transit of cyclonic events.

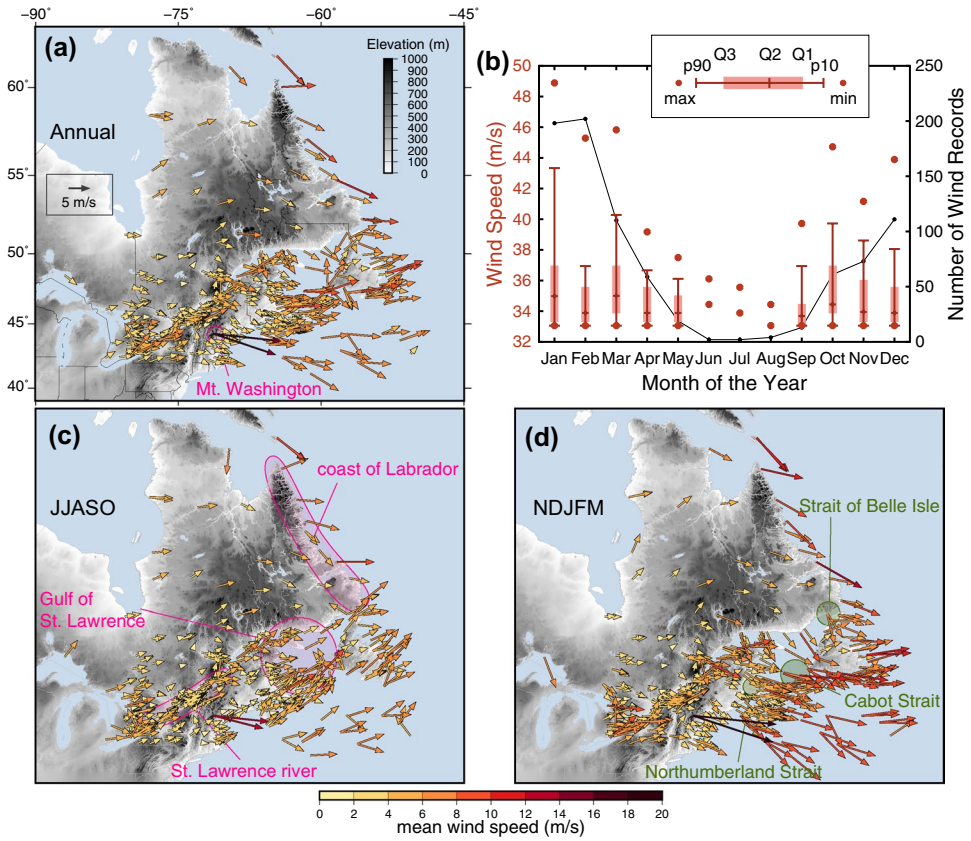

Fig. 1 **a** Mean wind speed of the original $WNENA_{ori}$ database with 525 sites. The mean wind speed is given by the color code and length of the arrow. The topography is given in grayscale. **b** Box and whisker plot of monthly distribution of wind speed records larger than 33 m s^{-1} (red); monthly distribution of events larger than 33 m s^{-1} in $WNENA_{ori}$ (black lines). **c**, **d** are the same as **a** but only taking in account JJASO and NDJFM months respectively. Some of the most important geographical features mentioned throughout the text have been highlighted in the maps

These cyclones can be either from tropical (Hart and Evans 2001) or, more commonly, from extratropical origin (Plante et al. 2014), that, in combination with topographical effects (Stewart et al. 1995), make this region also prone to the occurrence of extreme wind events.

Some aspects of the wind variability in this region have already been studied. Klink (1999a, b) analysed the linear trends of monthly maximum and minimum historical observational wind speed, and also the climatological mean and interannual variance of monthly mean wind speed, direction and velocity (the mean resultant vector) over the coterminous United States. Also for this region, Pryor et al. (2009) conducted an intercomparison of historical wind speed linear trends based on observational data sets, reanalysis products, and RCMs. Similar analyses on wind speed linear trends have also been conducted in Canada, as for example the work done by Wan et al. (2010) who previously developed a homogenization procedure to detect and correct systematic biases at the monthly scale. Also in Canada, Cheng (2014) analysed the historical trends of hourly wind gust observations and conducted future projection analyses (Cheng et al. 2014) of hourly and daily gust observations based on SD methodologies. Booth et al. (2015) studied the association between wintertime high-wind events in the northeastern United States, derived from observational daily wind maxima, and the path of extratropical cyclones, derived from 6-hourly sea level pressures (SLP) obtained from reanalysis data.

Additionally, as wind energy production has been gaining track in the region, with USA and Canada being among the world leading wind power producing countries (Wiser and Bolinger 2016), wind resource assessment studies have also been undertaken. Pryor et al. (2012) analysed past and future wind climates over the contiguous USA through a RCM model that fed from different reanalysis data and GCMs, and compared them to observations and regional reanalysis data. Martinez et al. (2013) developed a wind atlas over the Gaspé peninsula (located in Atlantic Canada) combining SD and DD methodologies that related reanalysis data, RCM outputs and 6-hourly wind speed and temperature observations. Despite these previous studies, there are still unexplored aspects regarding the variability of wind over the region of northeastern North America. To our knowledge, there have been no previous attempts to analyse the long-term climatological variability in relation with the large scale circulation patterns that govern this region.

In this work we analyse the multidecadal to centennial regional and local wind behaviour through the relationships between large scale atmospheric circulation patterns and the local surface wind. These relationships are obtained via a SD methodology based on the application of Empirical Ortogonal Functions (EOF) and Canonical Correlation Analysis (CCA). This SD methodology has been applied before with variables such as precipitation (e.g., González-Rouco et al. 2000; Hertig et al. 2012) and temperature (e.g., Xoplaki et al. 2003; Wójcik 2015) and also it has been previously implemented for wind related variables (Kaas et al. 1996; García-Bustamante et al. 2011, 2012).

The purpose of this methodology is twofold. On one side it identifies main circulation patterns (CCA patterns) governing the flow over the region and their associated time evolution (Canonical Series or CS). On the other side, the established statistical relationships with this methodology offer the possibility to estimate the local wind, hence the downscaling aspect of the technique. These estimations provide an uninterrupted timeline at each location. Such continuous time series are unfortunately not always available for surface observations (predictand field) due to the plethora of potential problems that can affect the measurements (e.g. Lucio-Eceiza et al. 2018a, b). An additional advantage is that, as long as we assume that these statistical relationships are also valid in the past, the time series can be extended back in time as far as there is availability of predictor data. This enables the reconstruction of the wind behaviour for longer time periods beyond that of the observational set.

This work presents a detailed description of the main governing large scale patterns over the region and an estimation of the local wind based on the obtained large-to-local scale relationships. It also describes the long-term variability of the large-to-local coupled patterns and shows the multidecadal to centennial behaviour of the reconstructed regional wind with the help of 20th century reanalyses and historical databases.

Inherent to all downscaling methodologies are the associated uncertainties that are propagated through the established relationships between the large scale and local information. A fundamental level of uncertainties is related to the choice of one SD technique over another (e.g., Zorita and von Storch 1999; Huth 2002; Jakob Themeßl et al. 2011). Other uncertainties depend on the methodological intricacies of each particular technique, linked to the somewhat arbitrary choice of certain decisions (e.g. Fowler et al. 2007) such as the variable used as predictor fields (e.g. Cavazos and Hewitson 2005), the size of the spatial domain used for the prediction (e.g. Benestad 2001) or the period used for the statistical calibration (e.g., Wu et al. 2016) among many others. Finally, another series of uncertainties are related with the sources of the chosen predictor(s) which can be variables simultated by GCMs (Najac et al. 2009), RCMs (e.g., Pryor and Barthelmie 2014), or large scale observations provided by historical databases (e.g., Zorita and von Storch 1999), or as in our case reanalysis data (e.g., Culver and Monahan 2013). García-Bustamante et al. (2011, 2012) explored the sensitivity of wind related predictands to different methodological alternatives by applying a similar SD approach as herein. The current work represents an updated contribution

to such studies, offering a sensitivity analysis that evaluates the impact of varying methodological choices, including for instance the type, spatial extension and source of the predictors fields. This evaluation in the context of SD methodologies for wind estimates has not yet been done up to date.

The description of the observational database, large scale predictor fields and teleconnection indices is presented in Sect. 2. A description of the methodology and experimental set up for the evaluation of the methodological uncertainties is given in Sect. 3. Section 4 presents the main large scale and local coupled circulation modes governing our region of interest. The sensitivity to changes in the reference configuration is explored in Sect. 5 where an evaluation of the wind estimates with an optimal (in a sense to be defined) SD configuration is also presented. The differences, similarities and characteristics of all predictor sources are also discussed here. In Sect. 6 we extend our knowledge of the wind variability in the region back to the 19th century using a set of available large scale predictors obtained from the different reanalysis and historical gridded datasets. We also propose an exercise that explores the relationships between monthly wind speed averages and hourly extremes by means of the presented SD methodology. The summary and conclusions are given in Sect. 7.

2 Data

2.1 Observational wind data, predictand

The present study is centred in the region of Northeastern North America, where an observational surface wind database that originally integrates 525 sites (Fig. 1a) was developed in Lucio-Eceiza et al. (2018a, b). It consists on 486 land stations distributed over Eastern Canada and five northeastern states of USA, as well as 40 buoys distributed between the East Coast and the Canadian Great Lakes. The dataset ($WNENA_{ori}$ hereafter) starts in 1953 and ends in 2010, spanning almost 60 years of hourly, 3-h and 6-h wind speed and direction records. $WNENA_{ori}$ has been compiled from various institutional sources and subjected to an exhaustive quality control process that, among other procedures, also involved height standardization for wind speed records and wind vane bias corrections. More detailed information on the compilation and quality assessment can be found in Lucio-Eceiza et al. (2018a, b). The current SD exercise uses zonal and meridional winds as predictand field, as they have shown better results over using wind speed alone (Curry et al. 2012; van der Kamp et al. 2012).

Figure 1a shows the spatial distribution of the mean wind speed and direction over the region of interest. The region evidences the orographic influence, channelling or redirecting surface wind, as exemplified by the channellings along the St. Lawrence river and the straits of Belle Isle, Cabot and Northumberland to name but a few. The mean winds, predominantly westerlies, reach their maximum values of up to 11 m s^{-1} along the coast of Labrador, the island of Newfoundland and the gulf of St. Lawrence. Notably high mean wind can be appreciated over the top of Mt. Washington (New Hampshire, 1917 m asl, with winds of up to 16 m s^{-1}). As indicated in the introduction, the geographical location of this region favours the transit of cyclones from tropical and extratropical origin. These configurations are more frequent and of higher intensity during wintertime (Wang et al. 2006), favouring a larger number of extreme wind events (see monthly boxplots of extreme wind records in Fig. 1b; e.g. Richards and Abuamer 2007). As it can be observed in Fig. 1c, average wind speeds during the extended summer season (JJASO months) are sensibly lower compared to winter (Fig . 1d, NDJFM). Enhanced associations between the synoptic circulation and the local variability can be expected on the basis of higher wind speeds and larger spatial variability, therefore these exercises focus on the NDJFM months. The analysis is focused on monthly averages.

Although the observational database spans from 1953 to 2010, the length of the period for the downscaling exercise has been reduced. Missing values in the records can generate instabilities and adverse effects in multivariate analysis such as Principal Component Analysis (PCA; Jiménez et al. 2008). In order to maintain an adequate temporal representation that minimizes the number of gaps and at the same time present a homogeneous spatial distribution of sites, the period has been narrowed down to 1980–2010, our calibration period. A subset that comprises 95 sites that present at least a 50% of valid data during that period (Fig. 2a, $WNENA_{SD}$ henceforth) is kept. Nevertheless, even if $WNENA_{SD}$ is used to calibrate the SD methodology, $WNENA_{ori}$ will be used herein to provide a more comprehensive spatial representation in specific cases. Figure 2b shows the regional average of the zonal and meridional wind components of $WNENA_{ori}$ during the NDJFM season for the complete period; 1980 is highlighted as the beginning of the calibration period. Both components exhibit notable variability at interannual (e.g. 2–4 years) and decadal timescales. Both wind components exhibit positive long-term linear trends of similar magnitude during the 1953–1980 period (0.18 m s^{-1} dec^{-1} for U and 0.14 m s^{-1} dec^{-1} for V), that however, present opposing behaviours during the most recent 1980–2010 period (-0.07 m s^{-1} dec^{-1} for U and 0.01 m s^{-1} dec^{-1} for V). Nevertheless, confidence is low on them as they can be affected by the decreasing number of available sites before late 1970s, in fact, none of these trends are statistically significant ($p < 0.05$); the variability during that interval is also higher possibly due to the lower number of operating stations (see black line in Fig. 2b). Similarly, the trends during 1980–2010 are also statistically non-significant.

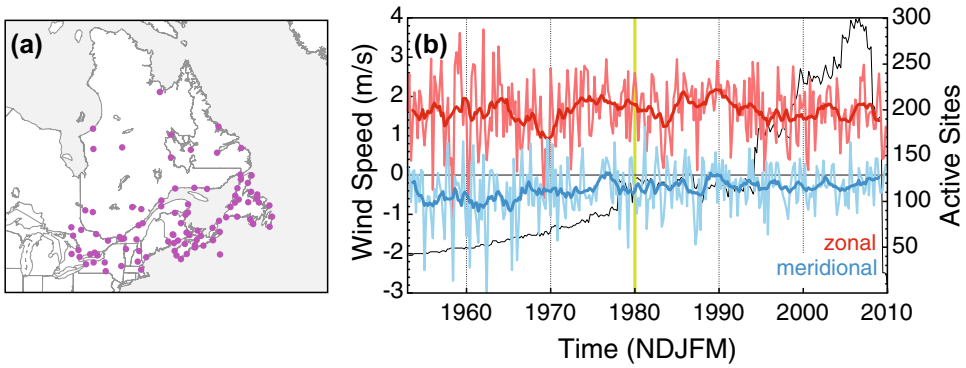

Fig. 2 **a** Spatial distribution of the 95 selected sites for the statistical downscaling process ($WNENA_{SD}$). **b** Regional mean (left y axis) of NDJFM monthly zonal (red) and meridional (blue) wind for $WNENA_{ori}$. The thicker lines correspond to a 10-month centred running mean (i.e. 2 year low pass filter). The number of active sites at any month are indicated with the black line (right y axis). The beginning of the calibration period (1980) is marked with a vertical green line

2.2 Large scale predictors

For the SD exercise, six variables have been used as predictor fields (Table 1): sea level pressure (SLP), 850 and 500 hPa geopotential height (Z_{850} and Z_{500}), 10 m height or surface level meridional (U) and zonal (V) wind components, and 500-850 hPa thickness (ΔZ). All the variables are at monthly resolution and have been obtained either from all the current twelve global reanalysis products or from two additional observational gridded databases (Table 2).

Each global atmospheric reanalysis has a different time length (Table 2): six reanalyses cover a period similar to our SD exercise period (~ 1980 to 2010); three reanalyses span until approximately the beginning of our observational database (~ 1950 to 2010) and three more cover the whole 20th century or even further back up to the mid 19th century, which allow us to expand this analysis up to mid 19th century. Most of the reanalysis products are based on atmospheric models, except for CFSR, originated from a coupled atmosphere–ocean–sea-ice model, and Cera-20C, based on the coupled ocean–atmosphere model used at the ECMWF. Additionally, Cera-20C and 20CRv2c comprise an ensemble of 10 and 56 members respectively, although for this exercise only the ensemble mean has been used. The spatial resolution of the reanalysis products ranges from 0.5°× 0.5° to 2.5°×2.5°. The majority of them assimilate a great number of variables (e.g., SLP, temperature, wind, radiation) from conventional observations (e.g., ships, buoys, radiosondes, dropsondes, aircrafts, profilers, land sites) and satellites, although there are some exceptions: JRA55C only assimilates conventional data, and the 20th century reanalysis products (Era-20C, Cera-20C, 20CRv2c) only assimilate SLP and sometimes surface marine wind data as well. None of the reanalysis products assimilate surface wind from land sites (Uppala et al. 2005; Onogi et al. 2007; Dee et al. 2011; Ebita et al. 2011; Rienecker et al. 2011; Kobayashi et al. 2014; D. Schuster 2016, personal communication), thus assuring statistical independence with $WNENA_{SD}$. Please, refer to Table 2 for a concise description of these reanalysis products. A comprehensive side-by-side intercomparison between most of the global reanalysis products used herein can be found in Fujiwara et al. (2017); Torralba et al. (2017).

Two independent instrumental SLP datasets are additionally used: ds010.0 (1899–present time; CISL RDA 1979) and HadSLP2r (1850–2012; Allan and Ansell 2006, both with a 5°×5° resolution. HadSLP2r was obtained combining HadSLP2 (1850–2004) and HadSLP2r (2005–2012), the last one adjusted to have the same mean and variance as HadSLP2 (please refer to the webpage indicated in Table 2 for more information).

All different reanalysis products are used for the calibration of the statistical model allowing an analysis of the

Table 1 Characteristics of the variables employed as large scale predictors: variables considered within the dataset, data source, level and units

Variable	Source	Level	Units
Mean sea level pressure (SLP)	Observations/reanalysis	Surface pressure reduced to sea level	hPa
Zonal (U) and Meridional (V) wind speed	Reanalysis	10 m or surface level[a]	$m\ s^{-1}$
Geopotential height (Z)	Reanalysis	850, 500 hPa	m
Geopotential height difference (ΔZ)	Reanalysis	$\Delta Z = Z_{500} - Z_{850}$	m

[a]Surface level only for CFSR and 20CRv2c (summary of reanalyses in Table 2)

Table 2 Reanalysis and observational datasets used in this analysis: acronym, temporal coverage, spatial resolution used, number of vertical levels and height of top level, assimilation method, assimilated variables and useful references. The spatial resolutions that were interpolated at higher (lower) resolution than the original one are marked with $^{I}(^{i})$. Two type of assimilation methods are indicated, 3/4D variational (3/4D-var) and Ensemble Kalman Filter (EKF), over assimilation windows that range between 3 and 24 h. The assimilated observations mentioned are: conventional observations of multiple variables (CONV); satellite observations (SAT); surface marine winds (SMW); SLP; Sea Surface Temperatures (SST); and Subsurface Temperature and Salinity Profiles (STSP)

Name	Coverage	Spat. Res. (lat×lon)	Vert. Levs. (Top)	Assim. Method	Assim. Vars.	References
Reanalysis products						
Era-40	1957/09–2002/08	$0.75° \times 0.75°^{I}$	60 (0.1 hPa)	6-h/3D-var	CONV, SAT	Uppala et al. (2005)[a]
Era-Interim	1979/01–present	$0.75° \times 0.75°$	60 (0.1 hPa)	12-h/4D-var	CONV, SAT[1]	Dee et al. (2011)[a]
Era-20C	1900/01–2010/12	$0.75° \times 0.75°^{I}$	91 (0.01 hPa)	24-h/4D-var	SLP, SMW[2]	Poli et al. (2016)[a]
Cera-20C	1901/01–2010/12	$0.75° \times 0.75°^{I}$	137 (0.1 hPa)	24-h/4D-var	SLP, SMW;SST, STSP[3]	Laloyaux et al. (2016)[a]
JRA25	1979/01–2014/01	$1.25° \times 1.25°^{i}$	40 (0.4 hPa)	6-h/3D-var	CONV, SAT[4]	Onogi et al. (2007)[b]
JRA55	1958/01–present	$1.25° \times 1.25°^{i}$	60 (0.1 hPa)	3-h/4D-var	CONV, SAT[5]	Ebita et al. (2011)[c]
JRA55C	1972/11–2012/12	$1.25° \times 1.25°^{i}$	60 (0.1 hPa)	3-h/4D-var	CONV[6]	Kobayashi et al. (2014)[d]
MERRA	1979/01–present	$0.5° \times 2/3°$	72 (0.01 hPa)	6-h/3D-var	CONV, SAT	Rienecker et al. (2011)[e]
NCAR-R1	1949/01–present	$2.5° \times 2.5°$	28 (3 hPa)	6-h/3D-var	CONV, SAT	Kalnay et al. (1996)[f]
DOE-R2	1979/01–present	$2.5° \times 2.5°$	28 (3 hPa)	6-h/3D-var	CONV, SAT[7]	Kanamitsu et al. (2002)[g]
CFSR	1979/01–2011/01	$0.5° \times 0.5°$	64 (0.266 hPa)	6-h/D-var	CONV, SAT[8]	Saha et al. (2010)[h]
20CRv2c	1851/01–2014/12	$2° \times 2°$	28 (2.511 hPa)	6-h/EKF	SLP[9]	Compo et al. (2011)[i]
Observational SLP datasets						
HadSLP2r	1850/01–2012/12	$5° \times 5°$	–	–	–	Allan and Ansell (2006)[j]
ds010.0	1899/01–present	$5° \times 5°$	–	–	–	CISL RDA (1979)[k]

Assimilated Variables

[1]Same type of data as Era-40

[2]Only SLP (ISPDv2.2 and ISPDv3.2.6) and SMW (ICOADSv2.5.1;Hersbach et al. 2015)

[3]Same data as Era-20C for the atmosphere; for ocean SST (HadISST2) and STSP (EN3)

[4]Same data as Era-40

[5]Data from Era-40 + Japanese Meteorological Agency

[6]Same non-satellite data as JRA55

[7]Similar data as NCAR-R1

[8]Nearly the same data as MERRA

[9]Only SLP (ISPDv2;Cram et al. 2015); monthly SST and sea-ice distributions as boundary conditions

Downloaded from

[a]http://apps.ecmwf.int/datasets/

[b]CISL RDA (2007, 2008)

[c]CISL RDA (2013)

[d]CISL RDA (2015b)

[e]http://disc.sci.gsfc.nasa.gov/mdisc/

[f]http://iridl.ldeo.columbia.edu/SOURCES/.NOAA/.NCEP-NCAR/.CDAS-1/.MONTHLY/datasetdataselection.html

[g]http://www.esrl.noaa.gov/psd/data/gridded/data.ncep.reanalysis2.html

[h]CISL RDA (2010)

[i]http://www.esrl.noaa.gov/psd/data/gridded/data.20thC_ReanV2c.html and CISL RDA (2015a)

[j]http://www.metoffice.gov.uk/hadobs/hadslp2/data/download.html

[k]CISL RDA (1979)

sensitivity of the SD approach to different predictor data sources (Sects. 4 and 5). The 20th century reanalyses (Era-20C, Cera-20C and 20CRv2c) and the century-long observational datasets will be used to assess the long-term variability (Sect. 6).

2.3 Large circulation indices

The canonical series (CS) resulting from the SD methodology applied have been correlated with all teleconnection indices in Table 3 in order to relate the identified

mechanisms with well known modes of circulation. These modes might have an effect in the area under investigation herein, extending to both Pacific and Atlantic basins.

3 Statistical downscaling methodology

The SD methodology applied in this work is mainly based on EOFs and CCAs. Before applying the SD, the original data are transformed to anomaly fields subtracting the monthly climatology to remove the deterministic component of the annual cycle. To avoid inflated correlations due to long-term trends, the time series are also detrended through a linear least square fit (Xoplaki et al. 2004). To compensate for latitudinal distortions due to the decreasing size of grid boxes, the predictors are weighted at each point by multiplying by the square root of the latitude (North et al. 1982). Additionally, to avoid methodological instabilities produced by disparate variance values at different sites/grid points, all the time series are initially normalized by dividing by their own standard deviation (García-Bustamante et al. 2011). This normalization process is then reversed once the EOFs and CCAs are obtained so they present physical units and not an otherwise adimensional field.

The detrended and normalized predictand and predictor fields are independently projected onto their own S-mode (Richman 1986) EOF space (González-Rouco et al. 2000). Exploring the predictor–predictand relationships using this data reduces noise as only the modes with maximum explained variance are retained, drastically diminishing the dimensionality of the problem. For that reason, the number of retained EOFs has an influence on the SD model: too few EOFs could lead to discarding modes with a significant signal, thus producing poorer predictions; too many EOFs, on the other hand, could overfit the model to our particular dataset drawing us to an inadequate description of the underlying processes. This methodologies are further explained in von Storch et al. (1993). For cases with more than one predictor (multipredictors), the different predictor fields are merged previous to the EOF projection and jointly projected. The predictor and predictand EOFs are then introduced in the CCA model. The CCA methodology isolates the linear combinations of multiple predictor and predictand variables with optimum correlation coefficients, where the patterns are ranked according to their correlation values (e.g. Barnett and

Table 3 Description of the teleconnection indices: name, atmospheric variable on which the index is based on, short description and useful references

Index	Name	Variable	Description	References
AO (NAM)	Arctic oscillation (Northern annular mode)	SLP	1979–2000 monthly PC1 at 1000 hPa > 20°N	Thompson and Wallace (1998, 2000a, b)[a]
NAO	North Atlantic Oscillation	SLP	1899–2014 PC1 over (20–80N, 90W–40E)	Hurrell (1995)[b]
EA	East Atlantic	Z_{500}	1981–2000 standardized RPCA over NH	Barnston and Livezey (1987)[c]
EA/WR	Eastern Asia/Western Russia	Z_{500}	1981–2000 standardized RPCA over NH	Barnston and Livezey (1987)[a]
SCAND	Scandinavian pattern	Z_{500}	1981–2000 standardized RPCA over NH	Barnston and Livezey (1987)[c]
NP	North Pacific	SLP	Area–weighted over (30°N-65° N,160°E-140°W)	Trenberth and Hurrell (1994)[a]
PNA	Pacific North American Oscillation	Z_{500}	1981−2000 standardized RPCA over NH	Barnston and Livezey (1987)[a]
ENSO (Niño 3)	El Niño Southern Oscillation	SST	1981−2010 anomalies over (5°N–5° S,150°W–90°W)	Rasmusson and Wallace (1983); Cane (1986)[a]
SOI	Southern Oscillation Index	SLP	Tahiti *minus* Darwin standardized over 1981–2010	Trenberth (1984); Ropelewski and Jones (1987)[a]
PDO	Pacific decadal oscillation	SST	PC1 of monthly anomalies in North Pacific Ocean	Mantua et al. (1997); Yuan Zhang et al. (1997)[a]

NH stands for *Northern Hemisphere*, PC for *Principal Component*, RPCA for *Rotated Principal Component Analysis*

Downloaded from

[a]ESRL-NOAA Climate Indices List (http://www.esrl.noaa.gov/psd/data/climateindices/list/)

[b]NCAR-UCAR Climate Data Guide (https://climatedataguide.ucar.edu/climate-data/hurrell-north-atlantic-oscillation-nao-index-pc-based; National Center for Atmospheric Research 2016)

[b]Downloaded from CPC/NCEP-NOAA list (http://www.cpc.ncep.noaa.gov/data/teledoc/telecontents.shtml)

Preisendorfer 1987; González-Rouco et al. 2000). Once the large scale–local wind relationships are established, the local winds are estimated using the CCA patterns and the predictor fields (García-Bustamante et al. 2011, 2012).

In order to avoid spurious results due to overfitting (Barnett and Preisendorfer 1987), the skill of the SD is assessed using a crossvalidation approach where a small subset of data is dismissed in successive calibration and estimation steps and the model is evaluated with the retained data.

In a first step, a specific combination of model parameters is selected. This configuration, *reference* configuration hereafter (Sect. 4), does not necessarily correspond to the optimum case although it shows estimations that reasonably agree with the observations and illustrates the associations between predictor and predictand fields.

A methodological sensitivity analysis is also conducted, evaluating the sensitivity of the estimations to changes in five different methodological choices: (1) the size of the large scale domain, or window size, for the predictor; (2) the variable(s) used as predictor field; (3) the number of retained EOF/CCA modes; (4) the size of the crossvalidation subsets; (5) the reanalysis used for the predictor field.

For the window size, five possible domains are chosen (Fig. 3), each of them emphasizing certain possible large-scale connections such as the North Atlantic or North Pacific basin. The regression pattern of predictand's first PC over MERRA's SLP anomaly field is also presented to illustrate the spatial range of the large-scale modes in relation with the domains. Apart from the five variables used as predictors (Table 1, note that zonal and meridional wind are combined together as a single predictor variable), combinations of two and three variables are also considered, with up to 18 different predictor choices. The range of meaningful EOF modes is selected through the visual Scree Test method (Cattell 1966; not shown). The maximum number of selected CCA modes is imposed by the smallest retained number of EOFs between predictor and predictand (Barnett and Preisendorfer 1987), which cannot be exceeded. The number of retained $\text{EOFs}_{predictor}$/$\text{EOFs}_{predictand}$/CCAs ranges between 4/4/2–7/7/7 accounting for 62 possibilities. Finally, the size of the crossvalidation subset varies between 1, 2, 5 (a whole season or 1 *year*), 10 (2 years) and 20 months (4 years). Since only one parameter is changed at a time, we have 87 possible combinations for the sensitivity analysis per reanalysis, that is, 87×12 combinations in total. The ensemble is carried out using the *reference* configuration as the common base for each parameter. The results on the sensitivity analysis are given in Sect. 5.1. This procedure, although not as thorough, follows the approximation of García-Bustamante et al. (2011).

The predicting skill of the method with respect to the observations ($wind_{OBS}$, corresponding to WNENA_{SD}) is evaluated using five metrics: the standard deviation ratio (σ/σ_{OBS});

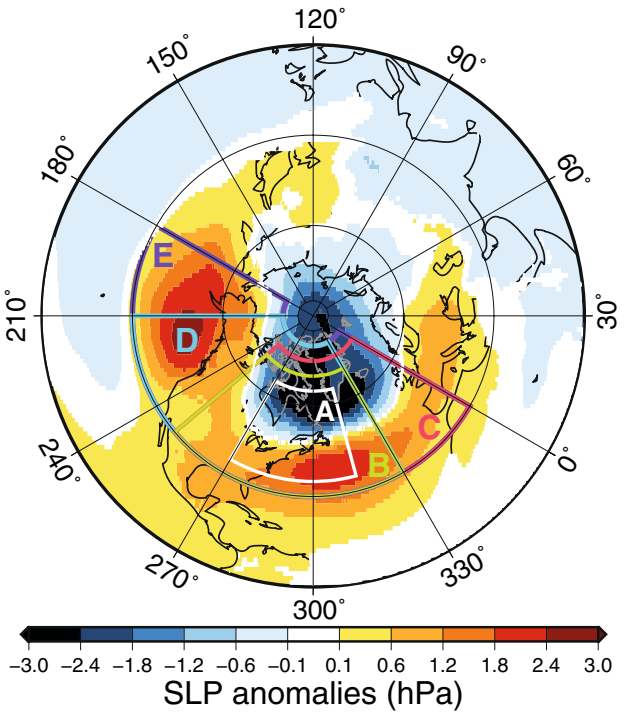

Fig. 3 The 5 different large scale domains (boxes) used as predictor windows in this work : A (35–65° N, 270–315° E); B (30–70° N, 250–330° E); C (30–75° N, 250–360° E); D (30–80° N, 210–330° E); E (30–80° N, 180–360° E). The regression pattern of WNENA_{SD}'s 1st PC over one of the predictor variables (MERRA SLP) used in the SD sensitivity analysis (Sect. 5.1) is shown in shaded colours

the normalized root mean square error (RMSE/σ_{OBS}); the Pearson correlation coefficient (r); the ratio of correlation absolute values of SD estimations ($wind_{EST}$) and reanalysis winds ($wind_{REA}$) respect to the observations ($|r_{(EST-OBS)}|/|r_{(REA-OBS)}|$); and the Brier Skill Score (von Storch and Zwiers 2003). Two versions of the Brier Skill Score have been used: β (e.g., García-Bustamante et al. 2011), and a modified Brier Skill Score, β':

$$\beta = 1 - \frac{MSE_{(wind_{EST} - wind_{OBS})}}{S^2_{wind_{OBS}}} \tag{1}$$

$$\beta' = 1 - \frac{MSE_{(wind_{EST} - wind_{OBS})}}{MSE_{(wind_{REA} - wind_{OBS})}} \tag{2}$$

β evaluates the skill of the SD estimated wind or the wind from the reanalysis relative to the observations, while β' evaluates the added value of the SD estimations vs. the reanalyses relative to the observations. $MSE_{(wind_{EST} - wind_{OBS})}$ represents the variance of the SD estimation error. $MSE_{(wind_{REA} - wind_{OBS})}$ represents the variance of the $wind_{REA}$ error. $S^2_{wind_{OBS}}$ is the variance of the observations respect to

its climatology, selected as a reference to evaluate the error. In such conditions $\beta \leq 0$ represents an estimation not better than climatology (or, for β', no improvement over $wind_{REA}$). $\beta > 0$ then represents an improvement over the climatology (or over $wind_{REA}$ for β'), where the better the SD estimation is, the closer is β (β') to 1. Taylor diagrams (Taylor 2001; Sect. 5.2, Fig. 10) are used to visually integrate the information about correlation, standard deviation and normalized RMSE in a concise way.

In the comparison of SD derived estimates and reanalysis products, the wind speed anomalies of the gridpoints closest to each observational site have been selected for the calculation of the metrics described herein.

The calibration and evaluation period for Sects. 4, 5 comprises the 1980–2010 interval, except for Era-40 that ends on 2002. The extended NDJFM winter season over this period gives a set of 145 monthly observations and constitutes an interval close to a Climatological Standard Normal (WMO 2011; the most recent one being 1981−2010).

4 Downscaling experiment: reference case

This section analyses the results of the *reference* configuration (see Sect. 3). This configuration uses the SLP field as predictor, a suitable single predictor for the surface wind field (e.g., García-Bustamante et al. 2011; van der Kamp et al. 2012). It retains four EOF modes from both predictand and predictor and three CCA modes. The chosen window expands from 30–70°N and 250–330°E (window *B*, Fig. 3). The crossvalidation subset length is one month.

Although all experiments in this section and the following ones have been independently run for all the reanalyses (Table 2), in the *reference* case only the canonical patterns and series corresponding to the MERRA reanalysis are shown. The election of MERRA is for illustrative purposes solely since, as it will be shown throughout this section, the arbitrary choice of one reanalysis over another does not significantly affect on the described modes of covariability, indicative of their very similar described underlying dynamics. The total variance accounted for by the retained first three CCAs is of 59.3% for the predictand and 55.3% for the predictor. The 4th mode presents a non significant ($p < 0.05$) canonical correlation. Figures 4, 5 and 6 present the CCA patterns (a), the CSs (b) and the normalized wavelet power spectrum of the predictor's CS (c). In the CCA patterns, the SLP anomaly field is presented with isolines. Additionally and for visualization purposes, the regression pattern of Z_{500} with the SLP predictor CS is also presented in color shades. Similarly, the observational wind anomalies are the regression patterns of the predictand's CSs over $WNENA_{ori}$, expanding from the original 95 sites used ($WNENA_{SD}$). Figures 4, 5 and 6d show the absolute correlation values between the predictors' CS and

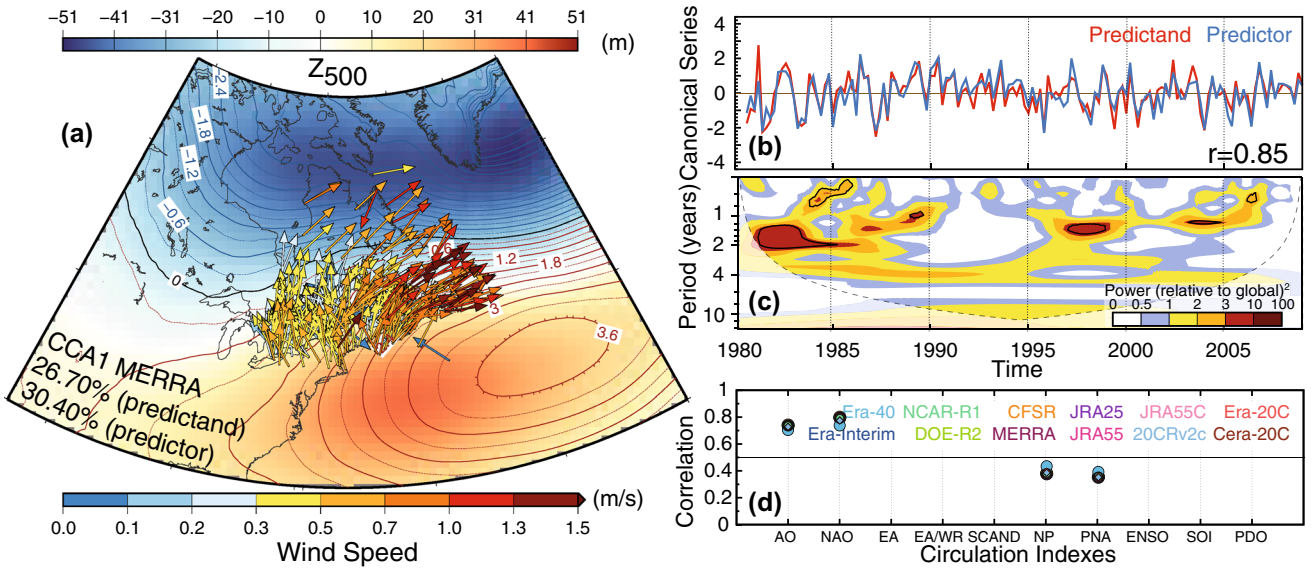

Fig. 4 **a** First CCA pattern (CCA1) using SLP as predictor for MERRA Reanalysis (isolines, hPa), the shadings correspond to Z_{500} (regressed pattern), and the vector field to the observational database (predictand). The wind speed is given with the color scale. **b** First CS of the predictor (blue) and predictand (red). The correlation between both is also provided. **c** Wavelet spectral power of the predictor's CS. The colours represent the normalized variances scaled by the global wavelet spectrum (Torrence and Compo 1998). The cone of influence, beyond which edge effects become important, is indicated with dashed lines. The black contour lines enclose the significant areas ($p < 0.05$), using a red-noise (first-order autoregressive) background spectrum. **d** Absolute correlation values between the first CS and different circulation indices. Colors correspond to different reanalyses. All correlations shown here are significant ($p < 0.05$)

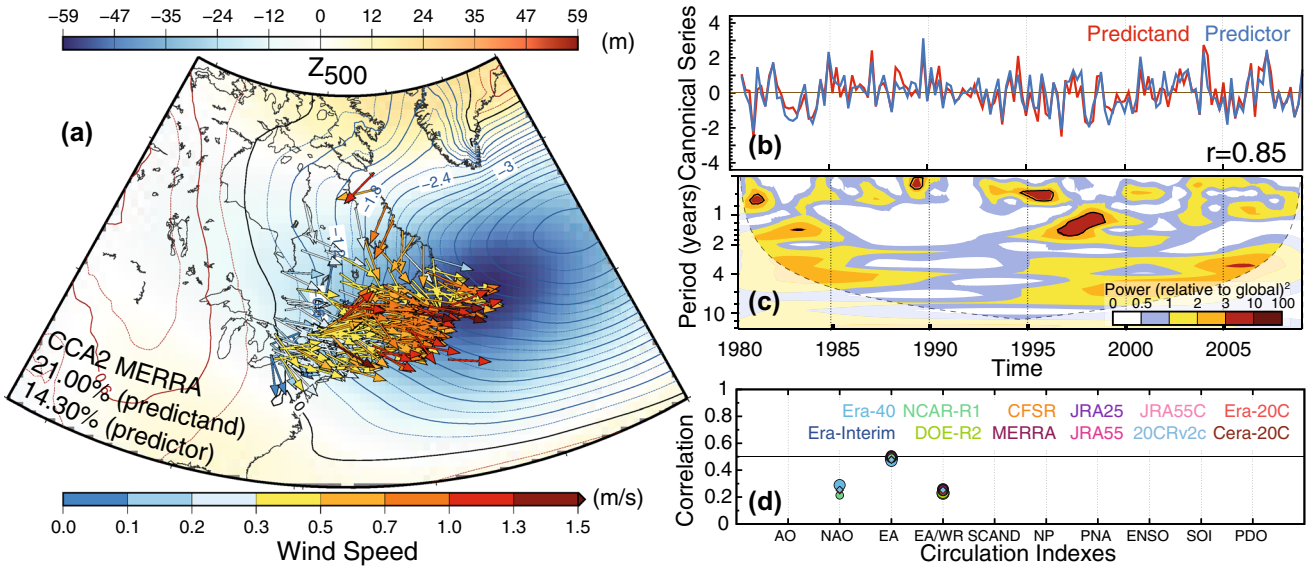

Fig. 5 As in Fig. 4 but for the CCA2 mode

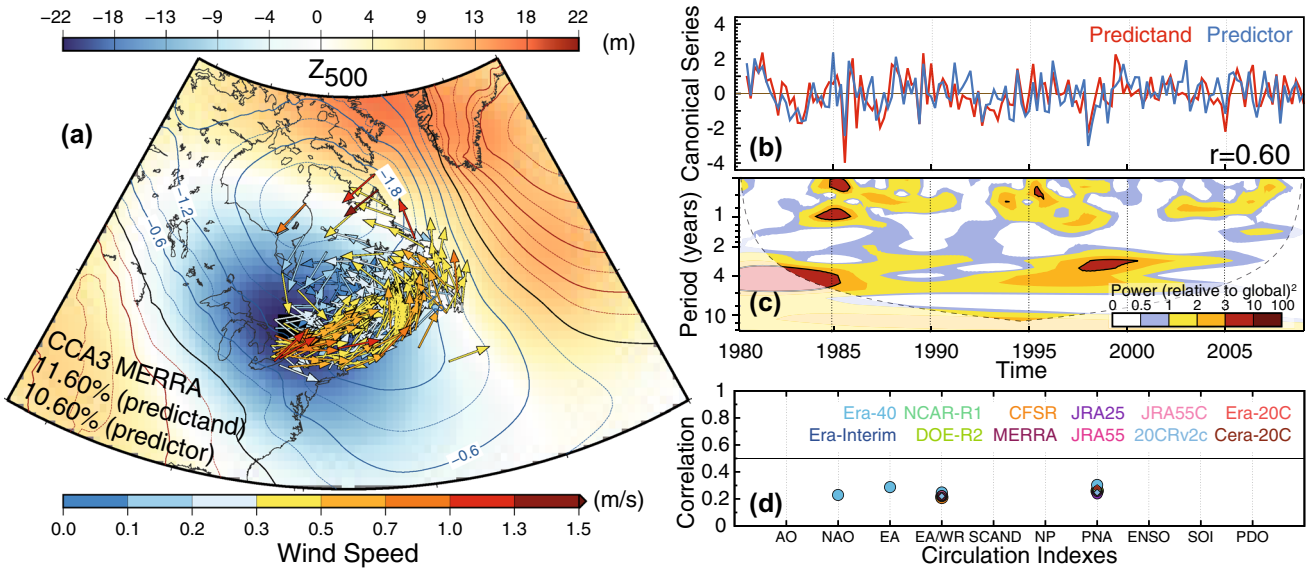

Fig. 6 As in Fig. 4 but for the CCA3 mode

the teleconnection indices presented in Sect. 2.3 (Table 3) for all the reanalyses (colors), offering information on how similarly they behave. Only the statistically significant correlations ($p < 0.05$) are presented.

The predictor field, SLP, of CCA1 (Fig. 4a), presents a zonal dipole structure with an equivalent barotropic structure of the Z_{500} field, with positive anomalies centred over the North Atlantic and negative anomalies centred between Greenland and Iceland, below the Denmark Strait. The western edges of the high reach the continent and favour S–N anomalous wind that become more zonal to the NE over Cape Breton Island. The CCA pattern of surface wind anomalies also shows a clockwise spinning structure, SW to NE, with higher wind speeds at the East Coast, specially along the coast of Labrador, Newfoundland and Nova Scotia, and a weaker response around Great Lakes and Ontario. As expected, wind anomalies deviate at the surface from the geostrophic balance, parallel to isolines, and from the high to the low pressures. The geographical channelling effect that takes place along the strait of Belle Isle (between Newfoundland and Labrador) is noteworthy, as well as the large wind anomalies of Mt. Washington (New Hampshire, see Sect. 2.1

and Fig. 1a, c, d), the largest ones in all CCA modes. The orographic and variability outlier that presents Mt. Washington is a practical example of the convenience of using correlations over covariances for EOF and CCA exercises. The positive phase of this coupled mode of circulation favours the flow of northerly cold and dry air masses originated in the continental Arctic, leading to colder than normal winters over the northeastern regions (Bonsal and Shabbar 2008). On the other hand, an intensification of this mode also displaces the polar jet, usually located below the Great Lakes, poleward of its climatological position (see regressed Z_{500} anomalies in Fig. 4a; Athanasiadis et al. 2010) deflecting the North Atlantic storm track northward and leading to dryer than normal months along the Labrador coast, Newfoundland and Nova Scotia. This first mode accounts for 30.4% (26.7%) of the total variance for the predictor (predictand).

The associated CS1s (Fig. 4b) show a correlation of 0.85. A large proportion of their spectral power is concentrated within the first decade, distributing in 1–2 year timescales, shifting to higher frequencies after 1995 (Fig. 4c). The 1990–1995 period shows the lowest variability with a persistent tendency to positive anomalies. The mean regional winds (Fig. 2) show significant ($p < 0.05$) correlation values of ~ 0.8 (0.5) between the CS1 and the regional meridional (zonal) wind components. As expected, this pattern is also the leading one, showing the highest correlation values with the regional winds and accounting for larger percentages of variance than the rest of CSs (not shown). The CS of the predictor shows relationships at different degrees with the main large scale teleconnection patterns that may affect the region (Fig. 4c). NAO (~ 0.8) and AO (~ 0.7) present the higher correlations, representing the most relevant circulation modes that dominate the wind variability in this region during wintertime (Ogi et al. 2003), as well as a strong contributor for the cyclone activity (Wang et al. 2006; Plante et al. 2014). The correlation values are very close between the different reanalyses, suggesting that their first mode describes similar dynamics regardless of the choice.

The positive phase of the second pair of CCA patterns (CCA2) and their associated CSs are shown in Fig. 5. The predictor field shows a center of negative anomalies over the central North Atlantic ocean. This configuration induces north/north easterly anomalies in the northern region of our area of interest. In the region between the west and New Brunswick and Main, the Canonical pattern of surface wind shows, consistently with circulation, westerly/north westerly anomalies. Towards Nova Scotia and Newfoundland the anomalies become more zonal following isolines and progressively crossing them as described in the first mode. This is the area with largest anomalies for this mode, a result of the combined effect of the large-to-local interactions and the geographical channelling between both land masses. Similarly to the positive phase of the CCA1, this configuration also favours the arrival of colder and dryer air masses from the continental Arctic causing overall colder and dryer winters than the climatological averages. This second mode accounts for 14.3% (21%) of the total variance for the predictor (predictand). The associated CSs (Fig. 5b) show a correlation of 0.85. This mode shows variability at lower (4–8 year) timescales than CCA1 and a decadal negative trend during 1985–1995. The CS of all the reanalyses show the largest positive correlation values (~ 0.5) with EA (Fig. 5c), a contributor on the cyclogenesis of the easternmost provinces of Newfoundland and Nova Scotia (Mailier et al. 2006) and one of the dominant modes of variability over the North Atlantic basin during wintertime (e.g.; Ulbrich et al. 2009; Athanasiadis et al. 2010). As it was the case with CS1, the results are also very similar for the different reanalyses.

Results for CCA3 are shown in Fig. 6. The predictor field shows a train of waves with negative anomalies over the center of Quebec and North of Gulf of St. Lawrence, and two positive anomalies located in SW–NE direction over central contiguous USA and Iceland respectively. The predictand field exhibits a counter clockwise pattern consistent with the low pressure over our area of interest. The highest wind anomalies are located in the outer border of the low center, over the Great Lakes, easternmost coastline and Labrador. Additionally the SW-NE channelling effect of the St. Lawrence river produces the highest wind anomalies, starting at the Lake Ontario all along until the mouth of the river. This configuration favours the flow of humid and warmer air masses inland resulting in wetter and warmer than average winters over most of the East Coast. This third mode accounts for 10.6% (11.6%) of the total variance for the predictor (predictand). The associated CSs (Fig. 6b) show a correlation of 0.60, although at lower frequencies the correlation is higher: 0.78 if a low pass moving average of 6 years (30 months) is applied. This mode accumulates most of the variability in timescales of to 4–5 years (Fig. 6b), similar to CS1. The CS shows positive low albeit significant ($p < 0.05$) correlation values with PNA a mode of variability that has been found to affect on the cyclone development and activity over the Great Lakes (e.g. Isard et al. 2000) , the region most affected by this CCA in general (Gulev et al. 2001; Grise et al. 2013). At lower frequencies (1, 2 and 4 year low pass filter outputs), CS3 shows higher negative correlation values with SOI and ENSO (~ 0.5 to 0.6, $p < 0.05$, not shown), a teleconnection pattern that has been previously found to affect this area (e.g., Plante et al. 2014). Like with CS1,2, the correlation values are, in general, similar for the different reanalyses and hence, also their underlying dynamics.

After the cross-validation, the estimated wind speed anomalies obtained from the *reference* case show a great accordance with the observations and among each other (Fig. 7). The correlations between the estimated and

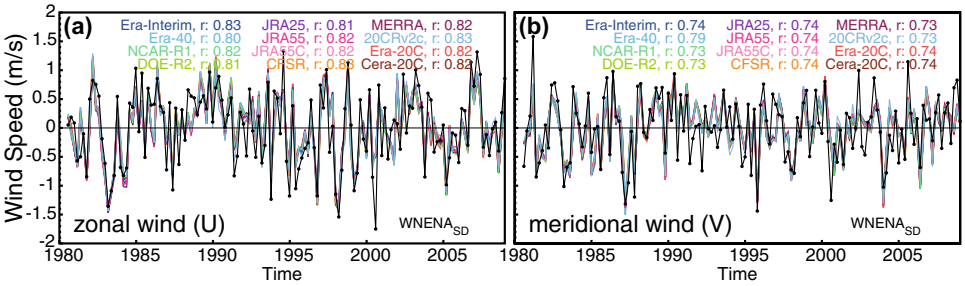

Fig. 7 Regional wind components time series obtained from the SD estimations with the *reference* configuration (color for reanalysis) and WNENA$_{SD}$ (black line) for **a** zonal and **b** meridional wind. The correlation values between the estimations and the observations are indicated for each reanalysis

observed regional anomalies for the zonal (a) wind component ranges between 0.80–0.83 and between 0.73–0.79 for the meridional (b) component depending on the chosen reanalysis (e.g. MERRA is 0.82 for U and 0.73 for V), all significant ($p < 0.05$). In general, the zonal wind component is lightly better estimated than the meridional one. The variance is underestimated in every case, a downside inherent to this type of SD procedures (e.g. Fowler et al. 2007), as the estimations are based only on the linear relationships between the observational database and the large scale circulation patterns. The reproduced variance, quantified by the standard deviation ratios between estimated and observed series, is still very high and better for zonal (0.85–0.87) than for meridional (0.79–0.83) winds (not shown).

Surface wind variability in NE North America is therefore, to a large extent, well estimated by large scale circulation changes that can basically be synthesized by three modes of variability as described by Figs. 4, 5 and 6. The negative phases of these modes control the occurrence of anomalies of opposite direction at the surface. The result is robust to changes in the predictor data sources in Table 2. This also applies to teleconnections with large scale circulation indices. Nevertheless, in spite of the stability of the relationships found, it is worth analysing the sensitivity of these results to changes in the details of the methodology. This allows for some assessment of the methodological uncertainty.

5 Wind estimations: methodological sensitivity assessment.

5.1 Sensitivity of wind estimations to model configuration

This section explores the sensitivity of the SD methodology to changes in five different parameter configurations: (1) window size; (2) the predictor field; (3) the number of retained EOF/CCA modes; (4) crossvalidation subset; (5) the reanalysis data used. In total, an ensemble of 1,044 possible combinations has been run (see Sect. 3).

The dispersion of the ensemble of estimations is obtained for each site (95 in total) and for U and V independently as in García-Bustamante et al. (2011). For each factor of variation, the dispersion for every time step is calculated as the difference between the maximum and minimum estimated wind speed of the ensemble (18 members for predictor changes; 62 members for EOF/CCA modes etc.). We also produce temporal averages of the dispersion series so that a single value is assigned to each site as a measure of its particular sensitivity to changes in the SD configuration. In this way we obtain four different sensitivity values for each site, variable (U or V) and reanalysis corresponding to the estimates of each of the four factors of variation: window size, predictor field, number of EOF/CCAs and size of the cross-validation subset. The spatial distribution of the sensitivities for MERRA reanalysis is presented in Fig. 8a, b for zonal and meridional wind anomalies. The diameter and color of the inner circle indicates the largest sensitivity value (in m s^{-1}) and the factor responsible for it. The outer circumferences are placed in order of relevance of the parameters from smallest (inner) to largest (outer, which corresponds to the one responsible for the largest one again). Their diameters are proportional to their associated sensitivity: the closer the radii, the smaller the differences in sensitivity between parameters.

The relevance of the parameters on the the zonal estimations (Fig. 8a) appear to be regionally distributed. The window size seems to have a particular impact around the Gulf of St. Lawrence and the EOF/CCA number dominates everywhere else, although the sensitivity values given by one or the other are generally close (not shown). As previously noted by Huth (2002), in general, the estimations improve with the introduction of more CCA modes (not shown), which incidentally involves a higher number of EOFs as well. The estimations also tend to improve with smaller window sizes (not shown). Exceptionally in Mt. Washington, the site that shows the largest sensitivity, the most relevant parameter is the choice of the predictor both for U and V wind anomalies. At an altitude of ~ 850 hPa, this site is more prone to be better represented with the introduction of predictors at higher levels. For meridional estimations (Fig. 8b) the EOF/CCA number dominates almost everywhere, except

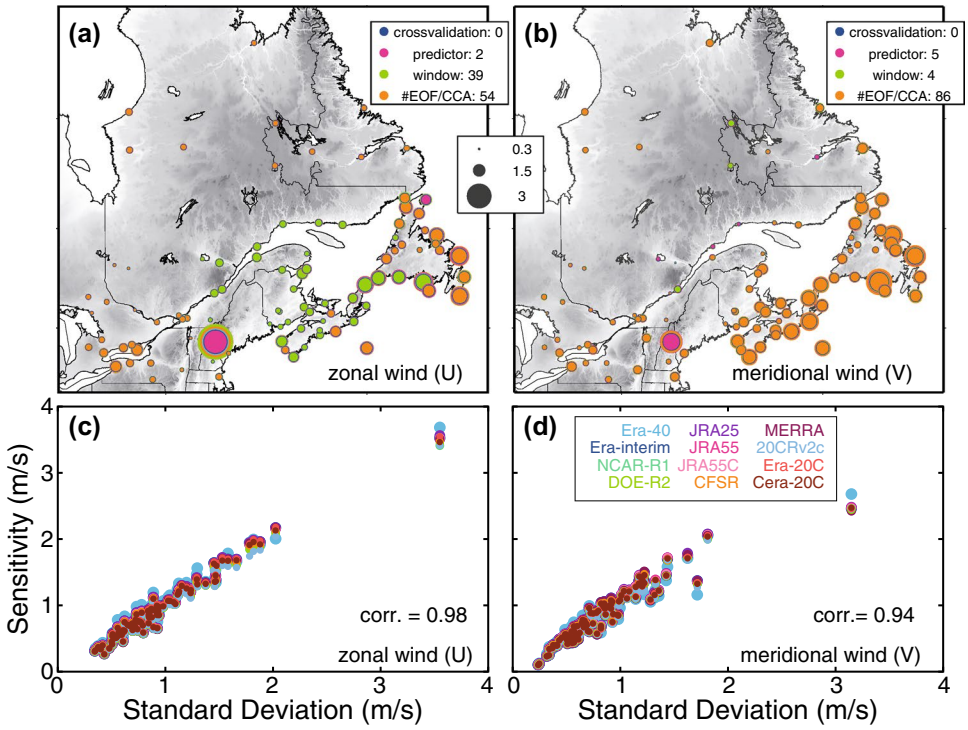

Fig. 8 Methodological sensitivity at each location for **a** zonal and **b** meridional wind to the change of one parameter of the SD reference configuration at a time. The parameter (filling color) that shows the largest sensitivity is depicted in the inner circle (see legend). The number of sites where each parameter is predominant is also indicated. The outer rings are proportional to the sensitivity shown by changing each parameter. These results are for MERRA reanalysis. Sensitivity vs. Standard Deviation at each site for **c** zonal and **d** meridional wind for each reanalysis (colors)

for a few places with zonal or SW–NE/NW–SE channellings where the choice of the predictor or window size is more important. These features are overall shared with all the reanalyses (not shown).

The regions with largest sensitivity values both for zonal and meridional winds are located over the windiest regions, by the shore, and in places with channelling effects (see Fig. 1d), where the wind variability is also higher. This relationship is shown by plotting the sensitivity at each site against its standard deviation (Fig. 8c, d), rendering a linear correspondence with mean correlation values (among all the reanalyses) of 0.98 for U and 0.94 for V. It is worth noting how closely do the estimated sensitivities at the sites behave for all the different reanalyses. The outlier value corresponds to Mt. Washington.

Figure 9 shows the sensitivity range for (a) zonal and (b) meridional wind estimations to the choice of the parameters and segregated according to the corresponding reanalysis. The very similar range of values for all reanalysis cases corresponding to each of the factors of variation is noteworthy.

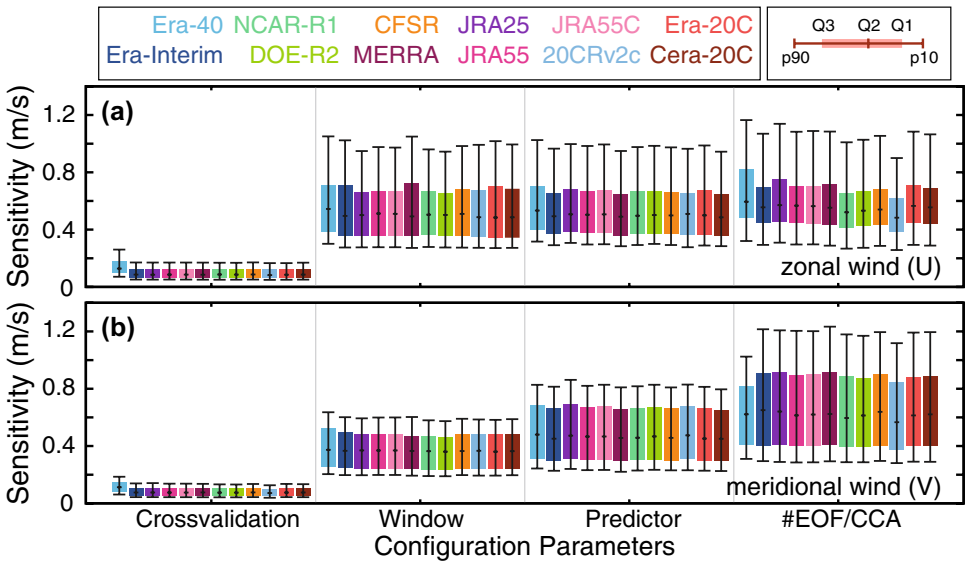

Fig. 9 Methodological sensitivity for each reanalysis for **a** zonal and **b** meridional wind to the change of one parameter of the SD reference configuration (Sect. 4) at a time. Each boxplot is constructed with the information from all sites. The reanalyses are color coded and the parameters are indicated in the x axis

Other authors also report a limited impact of using alternate data sources as predictors (Culver and Monahan 2013; Pryor and Barthelmie 2014). It is remarkable in Fig. 9 the small sensitivity of the wind estimates to changes in the size of the crossvalidation subset as indication that the CCA method is robust. In addition, the rest of parameters evidence very similar levels of sensitivity to variations.

An intercomparison exercise (not shown) between all reanalysis data sources performed for the first seven PCs, and repeated for different predictor variables, gives correlation values between reanalysis–reanalysis above 0.9 for the ensemble median at each PC. This suggests that the most relevant synoptic-scale information is equally captured by all reanalysis from coarsest to finest grid resolutions. Therefore, an increase on the resolution scale does not substantially improve the estimations as it does not contribute with additional valuable climatological information for its purpose at the large scale. Note that Era-40 spreads slightly different in Fig. 9 from the other reanalyses. This effect is likely due to the shorter calibration period used, since this reanalysis ends in 2002 instead of 2010. It is also worth noting that the sensitivity subjected to the choice of crossvalidation intervals is very small compared to the other parameters, an indication that the CCA methodology is statistically robust. In consistency with Fig. 8, the parameter with the largest values is the number of retained EOF/CCAs. For zonal estimations the sensitivity ranges of window size, predictor type and retained modes is very similar. The differences for meridional estimations are somewhat larger: the window size offers the lowest sensitivity, followed by the predictor type and ending with the number of retained modes that produces the widest range.

The previous results illustrate the low sensitivity differences of the SD estimations to the use of different reanalysis products as predictors, in contrast with the sensitivity presented to other factors. Given that some of the reanalysis products reach very high resolutions and detail in reproducing surface physics (e.g. CFSR and MERRA; see Table 2), the question arises therefore about how realistic their winds at gridpoints co-located to observations are in comparison to SD estimates.

5.2 Evaluation of the predictive skill for reanalysis wind and estimations

This subsection assesses the added value of our SD methodology in comparison with using the wind from the reanalysis products ($wind_{REA}$). We compare the parameter configuration that yields the best possible estimation in terms of its predictive skill with $wind_{REA}$, both regionally and site-by-site. One of the parameter configurations explored that offers the best predictive skill uses the UV field as sole predictor, the smallest window (A), 7/7/6 retained EOF/CCA modes and a crossvalidation subsampling interval of 1 month (henceforth denoted as *skillful* configuration). The total averaged explained variance is 76.6% (70.5%) for the predictand (predictor), ranging from 72.9–77.2% (66.9–73.1%) depending on the reanalysis source. Configurations with multiple predictors and a higher number of retained EOF/CCA modes have also been tried, obtaining a negligible improvement (not shown). We should bear in mind that a comparison between the SD estimation of the *skillful* configuration and the reanalysis data is advantageous for the SD, since it is using as predictors the $wind_{REA}$ themselves. This comparison can be argued to root in a traditional *Perfect Prog vs. Model Output Statistics* evaluation (von Storch and Zwiers 2003).

Figure 10 shows Taylor diagrams for SD estimations and reanalysis, both for the zonal and meridional components. The comparison shows results both for single sites (small dots) and regional averages (larger dots). The SD estimations (a, c) reproduce the observed local variability similarly regardless of the used reanalysis data. The standard deviation ratios (correlations) range 0.6–1.0 (0.6–0.9), although there are also a few sites with much lower correlations and ratios. The skill in reproducing the variance levels is slightly lower for the meridional wind component. The reanalysis winds (b, d) have, in general, higher correlation values in the range 0.70–0.97. The reanalysis meridional winds are also comparatively worse than the zonal winds. The greatest difference with respect to the SD estimations lays, however, on the ability to capture the variance of observations, as the standard deviation ratios change widely from below 0.5 to more than 3, depending on the site and reanalysis source.

The regional averages show correlations and ratios that depart from the centroid of individual sites, offering comparatively improved results. This is due to the fact that the regional averages can cancel out many local effects that in some cases are not well captured by the downscaling model (García-Bustamante et al. 2011). Both the SD estimated and the reanalysis winds have very high correlation values, above 0.95 ($p < 0.05$) for the zonal and meridional wind components. The regional variance is better reproduced by the SD estimations, with ratios of standard deviations between estimations and observations that range 0.97–1.01 (0.98) for zonal (meridional) wind speeds. Instead, the regional reanalysis winds show a very large range depending on the particular case: 0.91–1.75 (0.99–2.00) for zonal (meridional) wind components. While JRA55, JRA25 and MERRA show ratios that are close to 1.0, CFSR, 20CRv2c and specially DOE-R2 considerably overestimate the variance, specially for meridional winds.

Figures 11 and 12 offer a spatial comparison between the local skill of the SD estimations, of the reanalysis at the co-locate gridpoints and of both with respect to the observations. To better visualize the sensitivity of the simulated and SD estimated winds to the chosen reanalysis, we just show

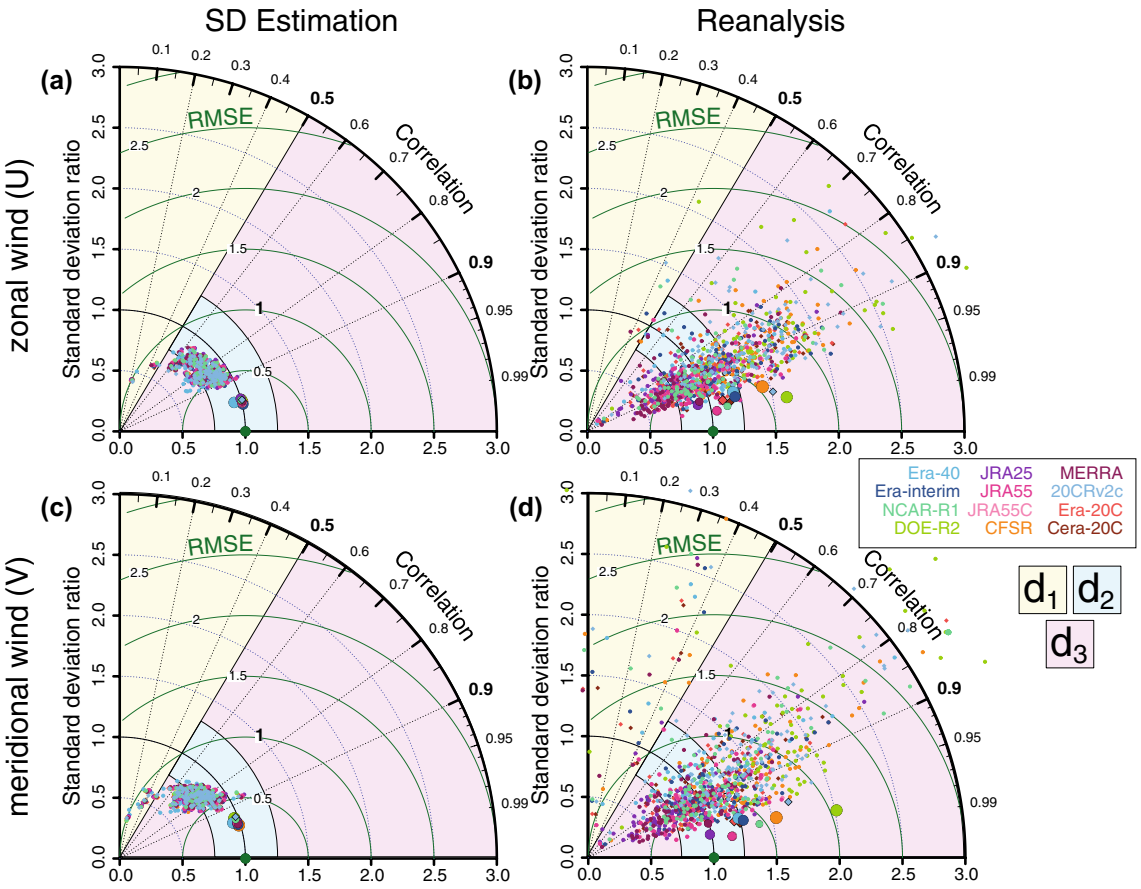

Fig. 10 Taylor diagrams constructed with the **a**, **c** SD estimations using the *skillful* configuration of Sect. 5.2 and **b**, **d** $wind_{REA}$ of all reanalyses (colors) with respect to the observations ($WNENA_{SD}$). In these diagrams the correlation values between SD estimations (or $wind_{REA}$) and $WNENA_{SD}$ are provided in clockwise angle scale, and the standard deviation ratios are given by the radial coordinate. The normalized RMSE values are indicated in concentric green circles. Each small dot corresponds to a particular site while the large ones depict the regional averages. **a**, **b** Show the results for zonal and **c**, **d** for meridional wind components respectively. Each Taylor diagram is divided in 3 domains according to correlation values and standard deviation ratios: domain 1 (d_1, light green) encompass sites with poor correlation values ($r < 0.5$); domain 2 (d_2, blue) comprises those with high correlation values and ratios ($r \geq 0.5$ and $\sigma_*/\sigma_{OBS} \in [0.75, 1.25]$, where σ_* is the standard deviation of either the SD estimations or reanalysis wind and σ_{OBS} that of observations). Finally domain 3 (d_3, light pink) corresponds to sites with good correlation but poor ratios. The geographical location of the sites at the (d_1, d_2, d_3) domains is shown in Figs. 11,12 for the case of JRA55 and DOE-R2 reanalyses

the wind from the reanalysis that compares better (worse) with the SD estimations, JRA55 (DOE-R2). Symbols at the leftmost and center columns show the results according to the three domains (d_1, d_2, d_3) identified in the Taylor diagrams of Fig. 10. The results of the SD estimations for both reanalysis sources are very similar (Figs. 11, 12, left column), as previously shown in the Taylor diagram. The correlations of the SD estimations respect to the observations are high ($r > 0.6$) for most of the sites. For zonal winds, the sites with the largest values are located in the eastern half the region. In addition to this, the majority of the estimations lie in d_2 showing a realistic characterization of the variance. The sites with worst estimations (d_1) are the same ones for both reanalyses, and correspond to places with complex orography such as mountain ridges, valleys or small islands.

The differences between the reanalysis winds in both reanalyses (center column in Figs. 11 and 12) are, unlike with the SD estimations, notorious. The reanalysis winds offer, overall, higher correlation values than the SD estimations (colors) although at the same time they tend to misrepresent the variance more frequently since their standard deviation ratios fall into the d_3 domain, specially for DOE-R2. The sites that present the lowest correlation values (d_1) are located, for both reanalyses, along the S–N channelled lake Champlain for zonal winds and along the St. Lawrence river and zonal channellings for meridional flows. The places where the variance is inadequately characterised (d_3) are, as expected, located in areas with intricate orography (marked valleys, fjords, coast sides). Here the reanalyses are unable to correctly resolve the surface winds as they have a coarse

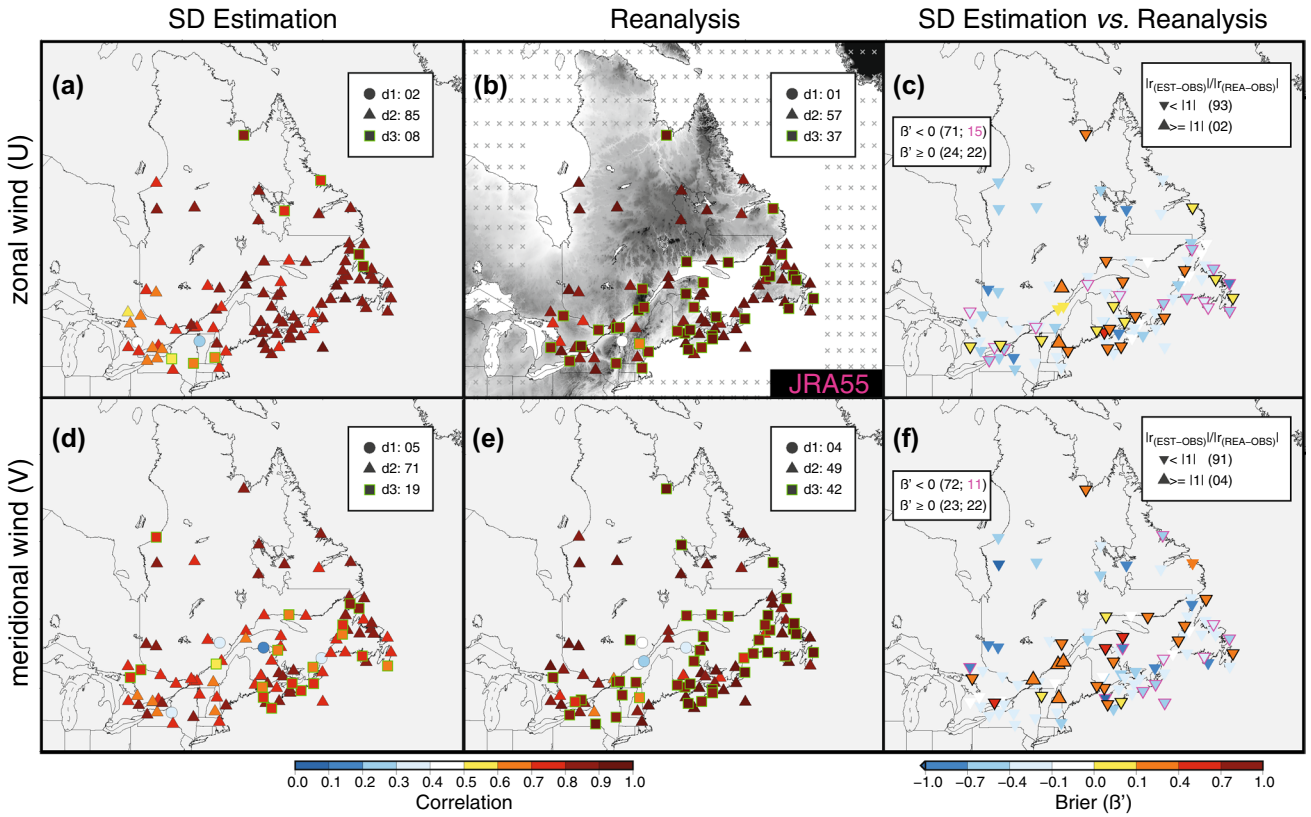

Fig. 11 Spatial representation of the correlation between the SD estimations using the *skillful* configuration in Sect. 5.2 (**a**, **d**) and $wind_{REA}$ (**b**, **e**), for zonal (top) and meridional (bottom) wind components using the JRA55 reanalysis both as predictor in the SD estimations and as direct reanalysis output at the gridpoints co-located to the observational sites. The gridsize of the reanalysis is indicated in **b**. The sites are classified in the three domains defined in Fig. 10 (d_1, d_2, d_3; see symbols). **c**, **f** Spatial distribution of β' values comparing the skills of SD estimations and reanalysis winds (color scale; Eq. 2). Regular (inverted) triangles indicate correlation absolute values between SD estimations and observations ($|r_{(EST-OBS)}|$) that are larger (lower), i.e. ≥ 1 (< 1), than correlations between reanalysis winds and observations ($|r_{(REA-OBS)}|$)

horizontal resolution (see the gridpoints in Fig.11b and 12b). This problem is specially pervasive in the case of DOE-R2, as it poorly represents the variability for the majority of the sites (squares).

Figures 11 and 12 (right column) offer a comparison of SD and reanalysis estimations for each observational site. Two parameters have been used for this task: the ratio of correlation absolute values ($|r_{(EST-OBS)}|/|r_{(REA-OBS)}|$); and the modified brier skill score (β', Eq. 2 in Sect. 3). In general, the correlation of $wind_{REA}$ is ubiquitously better (inverted triangles), except for a couple of NW-SE channelled valleys and Mt. Washington for zonal winds, and along the St. Lawrence river for meridional winds, where the reanalysis wind shows its lowest correlation values (Figs. 11e and 12e). The number of sites with correlation ratios ≥ 1 or < 1 stays relatively close for both reanalysis as they show very similar correlation values (Figs. 11 and 12, central column). Since, as seen earlier, the wind SD estimations also yield very similar results for both reanalyses, the values of β' will be then mainly dependant on how well the reanalysis reproduces the variance of observations, that as previously seen, varies greatly (recall Fig. 10). Indeed, the number of sites where the SD estimations perform better than the reanalysis winds (positive values) varies from less than 24% in case of JRA55 to more than 85% for DOE-R2. Despite these differences there are still some cases, triangles with borders in Figs. 11 and 12c, f, where the SD estimations have similar results for the exact same sites in both reanalyses. The sites where the SD estimations are better (worse) than the reanalysis winds are outlined in black (pink), and simultaneously belong to the d_3 (d_1 and d_2) domain in both reanalysis (Figs. 11 and 12, center).

As we have seen, SD estimations yield very similar results regardless of the chosen reanalysis, with high correlation values and realistic variance characterisations. Likewise, reanalysis winds offer similar and very high correlation values regardless of the specific product, outperforming the best SD model parameter configuration choice. On the contrary, the variance characterisation of reanalysis winds differs greatly from one case to the other. Thus, a site-by-site

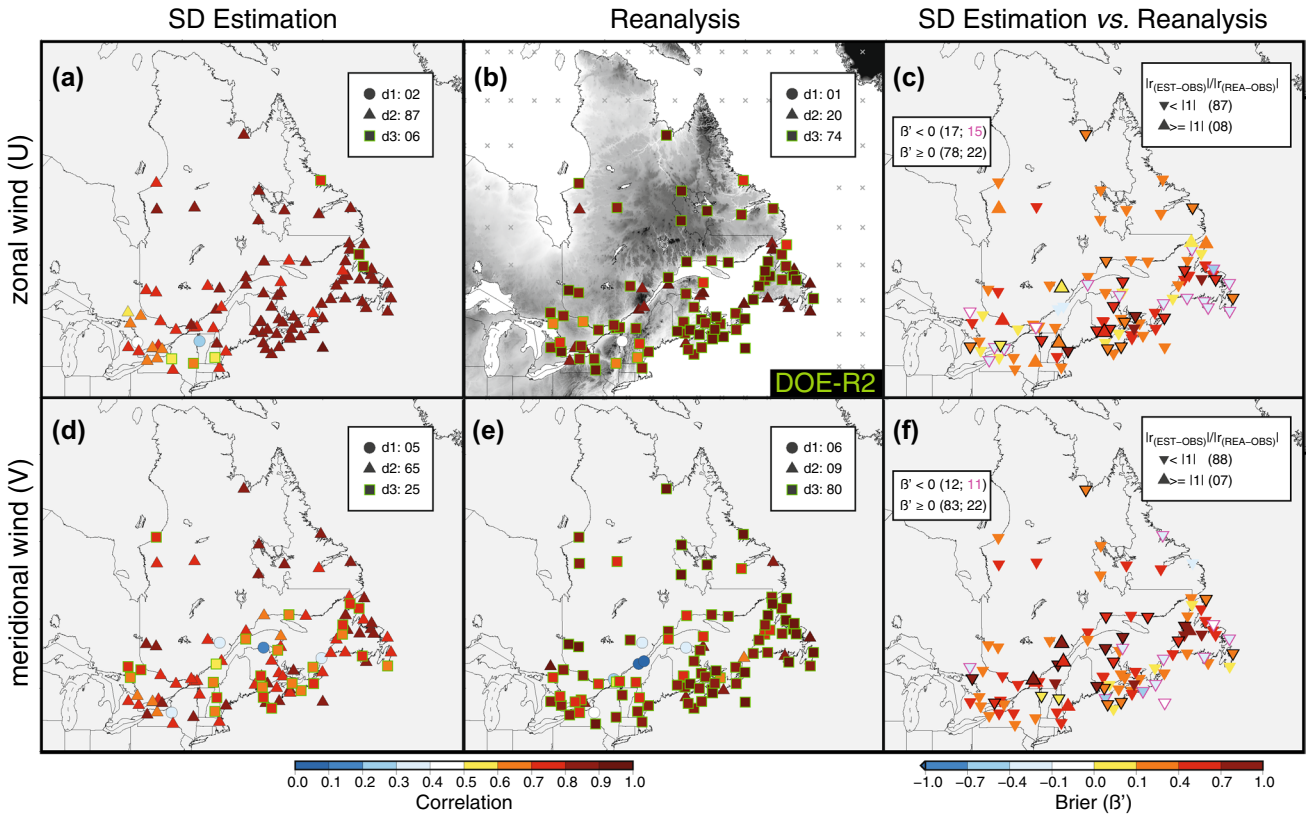

Fig. 12 As in Fig. 11 but for the DOE-R2 reanalysis

comparison between reanalysis and SD estimated winds is mainly dependant on the ability of the specific predictor source to reproduce the variance of the observations, with cases are the SD estimations are mostly advantageous (e.g. DOE-R2) and opposite ones (e.g. JRA55). Therefore one may ask which reanalyses offer the most and less realistic representations of surface wind speeds, and whether these behaviours are regionally or randomly distributed.

5.3 Reanalysis wind speed: an intercomparison of skill

We have shown in Sect. 5.2 that the model outcome from a SD with UV as predictor, or any additional predictor for that matter (see Fig. 9), is very similar regardless of the selected reanalysis source. On the contrary, the direct wind outputs from the reanalyses comprehend a wide range of standard deviation values depending on the particular case (Fig. 10b,e). As pointed out in Table 2, the reanalyses have very different horizontal grid resolution and assimilated variables. Additionally, some of them may be tunned to work better in certain regions of the globe and so their performance may vary regionally. For a side by side local comparison (Fig. 13), we have used the Brier Skill score (β, Eq. 1), as it allows for a measure of the explained variance, to select the best (a, b) and worst (c, d) reanalysis model for zonal (a, c) and meridional (b, e) wind components at each site.

JRA55 and JRA55C (JRA25, JRA55C, JRA55) show the best results for close to 40% (50%) of the sites for zonal (meridional) wind components, followed by MERRA, Cera-20C, Era-Interim and NCAR-R1 (MERRA, Cera-20C, Era-Interim). In many of the cases the β differences between the best performing reanalyses is very small. On another level, having higher resolution is no guaranty of improved performance over this area. For instance, the CFSR, being one of the newest reanalysis and having the highest spatial resolution, performs comparatively worse than first generation 2.5°×2.5° resolution NCAR-R1 and in 2/3 (3/4) of the sites ranks among the bottom half of all models for estimating U (V). The clustering of best model performance into subregions is noteworthy: JRA55 and JRA55C perform overall better in the North and the West, MERRA in the Gulf of St. Lawrence. For the worst performance (c,d) as expected, the older ERA-40, the only-SLP forced 20CRv2c and the low resolution DOE-R2, with 1/3 (2/3) the sites for zonal (meridional) speeds, behave comparatively poorly. The weak performance of DOE-R2 is mainly related to its overestimation of local wind variance (Fig. 12), which is usually linked to higher wind speeds (García-Bustamante et al. 2011). A reanalysis intercomparison exercise carried

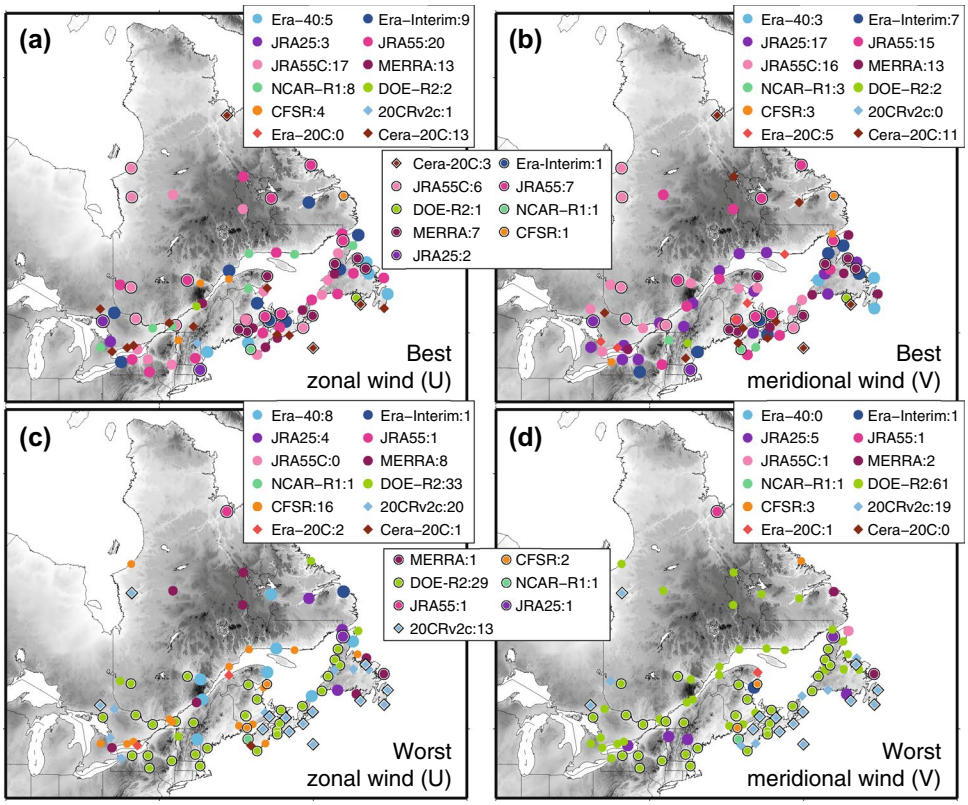

Fig. 13 **a**, **b** Spatial distribution of reanalyses (colors) whose corresponding wind outputs have the highest β values at each site for **a** zonal and **b** meridional winds. The sites where the best β corresponds to the same reanalysis for both U and V have a black border. **c**, **d** Same as before but for the reanalysis with worst β values. The legends indicate the number of sites for which each reanalysis performs best

out over the Arctic and conducted during the same period [1980–2009] showed a similar behaviour for DOE-R2 for the whole year round but specially in wintertime (Lindsay et al. 2014), which suggests that this might be a widespread problem. Surprisingly its predecessor NCAR-R1, outperforms DOE-R2 reanalysis almost everywhere, and shows more realistic variability values. DOE-R2 consistently performs the worst over North, West and Northern Gulf of St. Lawrence, and Era-40 and 20CRv2c over Nova Scotia and Southern Newfoundland.

It has been shown that, in general, both SD estimations and reanalysis wind perform well in this region. However, the SD estimations do not necessarily improve over the reanalysis direct wind outputs, as they only work consistently better over a minority of sites. Among the different reanalyses there is a wide range in terms of their performance in representing the observed wind, and they tend to cluster regionally. In some cases it can be argued why they perform worse, but in general the causes are not evident and go beyond the scope of the current work.

6 Wind climatology reconstruction

In the previous sections we have described the main large-scale patterns that govern the wind variability over our region (Sect. 4) and we have also carried out a sensitivity analysis on the predictability of the SD approach subjected to changes on the model scheme (Sect. 5.1). A reasonable strategy on this type of methodologies is to assume that the established predictor-predictand statistical relationship remain stationary in time (Zorita and von Storch 1999; Fowler et al. 2007). A long enough (of the order of decades) calibration period would cover manifold situations, including those of an altered climate. This assumption has been extensively applied in studies over future scenarios or past reconstructions (for precipitation e.g. González-Rouco et al. 2000; Frias et al. 2006; or wind e.g. Pryor et al. 2006; Cheng et al. 2014). Unfortunately there is no way of anticipating the temporal changes on these associations outside the observational period (García-Bustamante et al. 2011), a known drawback of the statistical models that has been pointed out in some studies (e.g. Hertig and Jacobeit 2014). Despite the known limitations, the assumption of stability can still help us to expand our estimations to reconstruct the past variability of our local wind observations from multidecadal (1980–2010) to centennial (1850–2010) timescales. For this exercise we project the whole length of the predictor anomalies from every reanalysis (see Table 2 for initial dates), calculated with respect to the calibration period 1980–2010, over the CCA patterns. Due to the fact that there are only three centennial reanalysis models we also introduce ds010.0 and HadSLP2r SLP gridded databases (Table 2), the longest gridded global SLP databases to our knowledge.

In a first step, we use the gained knowledge on the *reference* configuration (Sect. 4) to reconstruct the wind by using the leading 3 CSs. Afterwards, we also conduct a similar sensitivity analysis as in Sect. 5.1. We analyse the behaviour of the reconstructed regional zonal and meridional winds over a centennial period, and their associated uncertainties as well. Unlike before, however, we limit the predictor variables of every reanalysis to SLP, as is the only information provided by HadSLP2r and ds010.0. During this exercise we also disregard the crossvalidation subset size change, that was proven of almost no effect on the sensitivity analysis (see Fig. 9). However, the EOF/CCA number and window size are allowed to change, obtaining 310 possible parameter variations per source (62×5), that is, an ensemble of 4340 possible model configurations (310×14).

Figure 14a–c show the projected CSs from the three CCA patterns of the *reference* configuration. As it has been previously commented, all reanalyses resemble one another closely during the calibration period. The consistent behaviour holds back in time until the beginning of the first regular reanalysis model (NCAR-R1 starting at 1948). From 1948 back to 1850 only the century long reanalyses and the two SLP gridded databases are active. These five sources produce overall consistent results up until the 1920s, although some differences are apparent, specially in the second CS mode, where HadSLP2r shows some tendency towards a stronger eastward flux while ds010.0 and specially ERA-20C show a weakened or even reversed mode. The first evident discrepancies appear during 1900–1920, although they only manifest on the weakest mode, suggesting that there are only slight SLP field differences. These are very likely due to problems related to the gradual observational data scarcity during the database reconstructions (e.g., Allan and Ansell 2006) or during the assimilation processes that might lead to multiple inhomogeneities (among other problems, see Ferguson and Villarini 2014). As it seems, at least for the reanalyses, these differences are mitigated for the second half of the 20th century both for Era-20C and 20CRv2c (Wang et al. 2013; Befort et al. 2016).

The greatest discrepancies occur between HadSLP2r and 20CRv2c during 1860–1880, and they affect all three modes: while long-term trends can be appreciated in 20CRv2c, HadSLP2r shows an stable behaviour. This distinct behaviour is rooted on a positive regional bias of 20CRv2c respect to HadSLP2r that extends from the 1860s up to the mid 1870s (Fig. 14d), with differences reaching more than 6hPa at some dates (on the original monthly series, not shown). This bias is spatially distributed as shown in Fig. 14e, a zonally distributed dipole with its positive center (respect to HadSLP2r) located along the Hudson strait, between Labrador and Baffin Island, and a milder negative belt south of the Canadian border. To our knowledge there are no studies analysing the first two decades (1851–1871) of 20CRv2c, but it is reasonable to assume that this problem is more related with errors in the reanalysis rather than in the gridded database. On one hand, both the reanalysis and the gridded database show

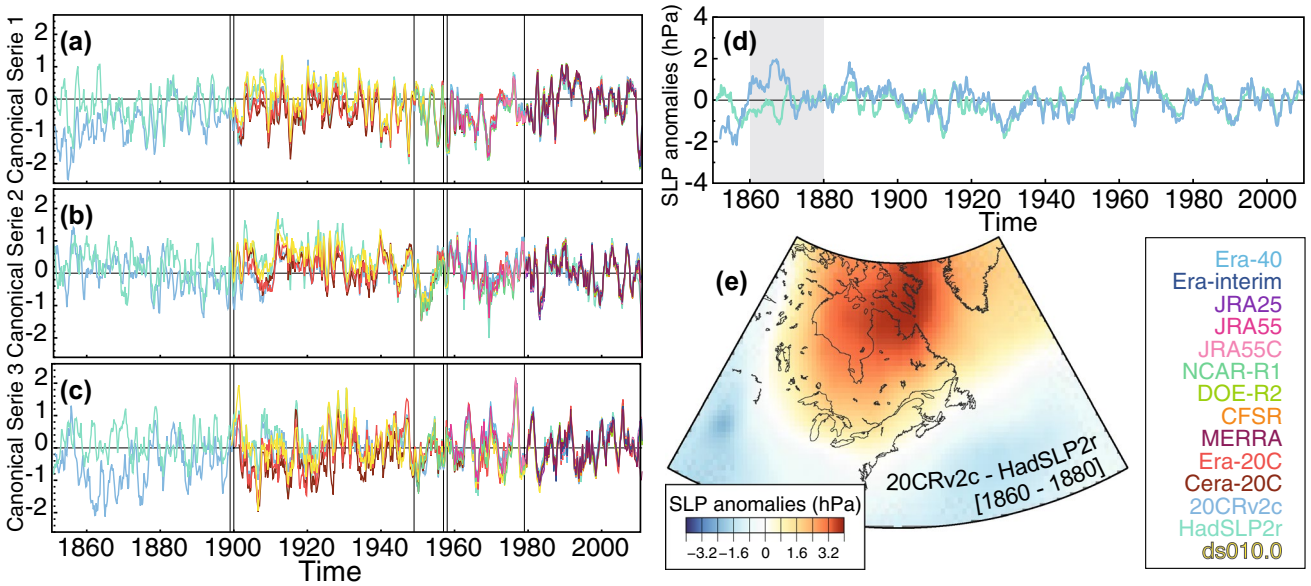

Fig. 14 **a** Extension of the first CS from the *reference* configuration (Sect. 4) to the whole temporal length of each reanalysis/database (inset, in colors). The series are 2 year low pass filter outputs. The vertical bars indicate the starting date of each reanalysis/database (see Table 2). **b**, **c** Same as **a** but for second and third CSs. **d** SLP anomalies of HadSLP2r and 20CRv2c over the region of interest. The anomalies are computed over the 1980–2010 calibration period and are presented as 2 year low pass filter outputs. **e** Differences between 20CRv2c and HadSLP2r SLP anomalies for the 1860–1880 interval. This interval is highlighted in grey in **a**–**d**

a good agreement back to the 1870s ($r = 0.91$, $p < 0.05$), but when they diverge afterwards they still show consistent variability at high frequencies. On the other hand, the CISL RDA (2015a) data sources report a low pressure bias in marine pressures from the US Maury Collection (Woodruff et al. 2005; Wallbrink et al. 2009) that affected variables like SLP from 1851 to about 1865. This bias is evident in Fig. 14d, and it can be speculated that there might be comparable problems on the subsequent decades as well.

The estimated regional zonal and meridional wind and their associated uncertainties (in deciles, shades of grey) are shown in Fig. 15a, b. The estimations obtained from the *reference* configuration are given in coloured lines as a guide, and the observational regional average is given in black thick line. The zonal wind appears to present a larger variability than the meridional wind. Both present variability on timescales over 20–40 years throughout most of the 1850–2010 period (see Fig. 15c, d, where the spectral analysis has been carried out with the median of the 4340 ensemble model outputs). The estimations during the observational period 1953–2010 follow very closely the observations. As it was previously described in Sect. 2.1, the meridional wind tends to gravitate over higher frequencies (2 years or less) while the zonal wind also shows timescales of 4 and 16–20 years. Through the 1950–1970s there is a marked 20 year timescale on the zonal component with a notably interannual high variability. This interval is primarily modulated by the second CCA mode (see Fig. 14b) and culminates with a brief period of very strong westward anomalies with a multi-decadal long negative trend that originates from the first CCA mode. The opposing effects of both modes on the meridional component produce an stable low variability southward flux during that time. This behaviour can also be interpreted (Wang et al. 2012) as derived from a strong NAO negative phase that extends from the 1930s to late 1970s in combination with a shorter period characterised by very zonal circulations fostered by an abrupt latitudinally alignment of its nodes. Conversely, a decades long NAO positive phase from the late 1890s to the 1930s (Hurrell 1995; Wang et al. 2012) produces a period of consistently positive westerly anomalies during that period. The uncertainty band, that keeps more or less constant since the 2010s, becomes notably wider before the 1880s. During this period, a bias on the 20CRv2c SLP field respect to HadSLP2r (Fig. 14d), with a configuration that resembles a negative NAO pattern, causes a notable strengthening of the westward (zonal) and southward (meridional) fluxes, departing from the estimations of HadSLP2r and consequently widening the ensemble uncertainty.

These results illustrate that there is not only interannual variability (1, 2, 4 year, Figs. 4, 5 and 6c) but also at the multidecadal scales (10, 20, 40 year) as well. It is important to note that this variability at longer time scales can be identified thanks to this reconstruction exercise, that extends our knowledge beyond of what we are allowed to see during the instrumental period. The multidecadal variability is larger and therefore significant in the context of the uncertainty. The trends indicated by the instrumental and the calibration periods are, thus, small and do not stand out in the multidecadal and centennial context.

We can observe that maximum values of surface wind components (Fig. 7) can be associated with situations in which the large-scale circulation modes that describe this region also reach maximum values of their CSs (Figs. 4, 5 and 6b). It is worth asking if any relationship can be drawn between the occurrence of very high winds in this region, specially during the winter months and usually associated with the passage of storms (Fig. 1b; Conrad 2009; Booth et al. 2015), and the phase of any of the large scale circulation modes. For this purpose we have used $WNENA_{SD}$ in its original, intra-daily resolution (Sect. 2.1; Lucio-Eceiza et al. 2018a), constructing a monthly series of wind maxima

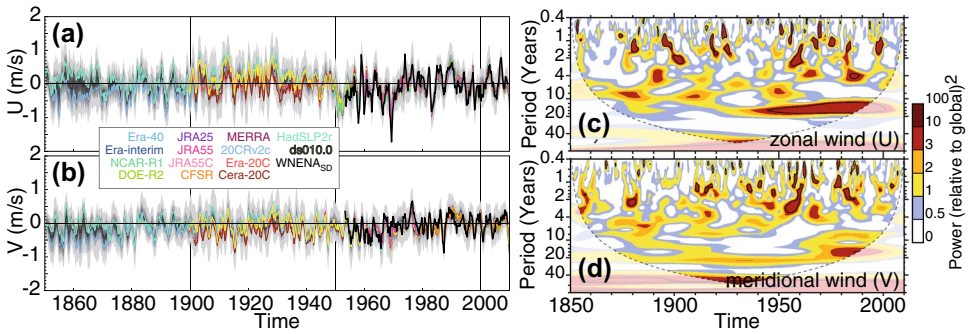

Fig. 15 Regional wind climatology reconstruction with its associated uncertainty (gray shading) for **a** zonal and **b** meridional wind anomalies. The observational database is presented with black lines. The sensitivity of the 4340 parameter configuration ensemble (310×14) is depicted in shades of greys for deciles, with the lightest grey for the maximum and minimum values. The *reference* configuration (Sect. 4) is given in colour for each reanalysis/ database (inset). The series are given as 2 year low pass filter outputs. **c**, **d** Wavelet spectral power (as in Fig. 4) of the ensemble median for **c** zonal and **d** meridional wind anomalies

for each site from the maximum ten minute speed measured during each month. The series of monthly wind maxima for each site and its monthly averages tend to be correlated (Fig. 16a), thus supporting that high wind values in some of the canonical modes may also be related to extreme wind behaviour. Figure 16b–d show the relationship between the monthly wind maxima anomalies obtained from a subset of $WNENA_{SD}$ with the values of each predictand's CS, corresponding to the *reference* configuration (Sect. 4). Each subset is formed with the sites that show significant correlations between their monthly wind maxima and monthly wind averages (Fig. 16a), and at the same time belong to the 25% of sites with largest absolute correlation values between their average monthly U or V anomalies and the corresponding CS at each case. The central values of the distribution of wind maxima anomalies for U and V are greater for maximum values of some of the CSs, that is, for situations in which some of the modes are more intense. This is especially true for both components in CS1 (Fig. 4a), and particularly for V in CS2 (Fig. 5a). There are no obvious relationships between monthly wind maxima and the third mode, however.

As seen before, the first mode of circulation is strongly related with the NAO/AO (Fig. 4d) whose positive phase favours the storm activity in central and Arctic Canada but diminishes the activity over the East Coast–Great Lakes area (e.g., Gulev et al. 2001; Wang et al. 2006). Consequently, some of the strong northeasterly wind speed anomalies from Fig. 16b, related to minimum CS1 values, might actually be attributed to the cyclonic activity over the region as they could favour the apparition of extratropical storms known as *nor'easters* or Northeastern snowstorms. These storms develop when cold air is delivered into the East Coast and encounters the warmer waters of the Atlantic Coast, moving then along the Atlantic seaboard (e.g., Hayden 1981; Conrad 2009). Although some of the strongest nor'easters can still form even under positive NAO conditions, in general is difficult to attribute the recorded wind speed maxima to storm activity under positive CS1 values. On the other hand, the northwesterly wind speed maxima related to positive CS2 conditions may have some relationship with the *Alberta clippers*, fast moving low pressure systems that originate east of the Rocky Mountains over the region of Alberta and travel southeast, sometimes reaching the East Coast (Conrad 2009). This phenomenon is usually related with dry, very cold and extremely windy situations (Thomas and Martin 2007) and when it reaches the Atlantic coastline can eventually develop in a secondary low, the aforementioned nor'easter (Zielinski 2002).

Despite the limitations that a linear SD methodology like this one has for capturing all the variability and specially extreme situations (e.g. Wilby et al. 2004), some relationships can still be established between high frequency phenomena and monthly modes of circulation that describe the behaviour on climatological timescales.

7 Conclusions and discussion

In this work we analyse the surface zonal and meridional wind behaviour over the area of Northeastern North America with a Statistical Downscaling model based on EOF and CCA techniques, identifying the major large scale

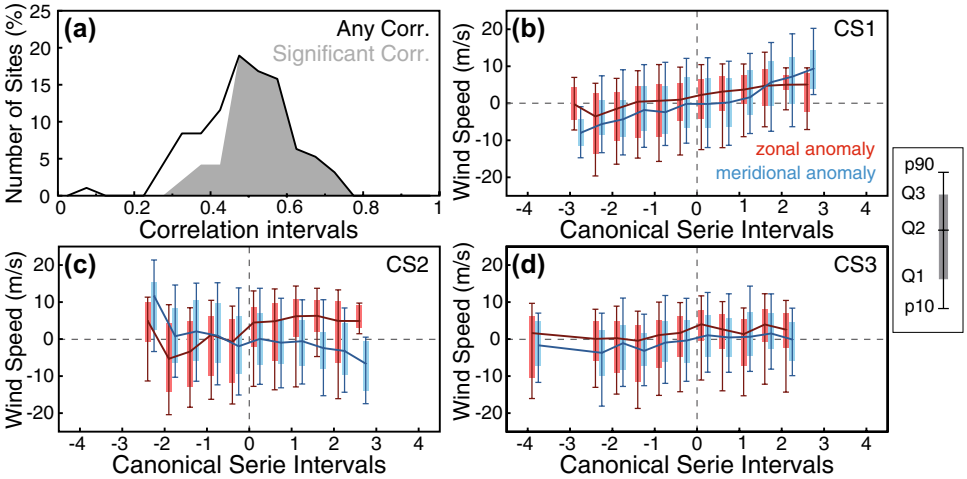

Fig. 16 **a** Number of sites (in %) from $WNENA_{SD}$ within each correlation interval, calculated between the monthly maxima and average wind at each site. The distribution of sites with significant ($p < 0.05$) correlations is shaded. **b** Box–and whisker plots of the distribution of monthly wind maxima anomalies of U (in red) and V (in blue) recorded at any time by a certain subset of sites vs. the corresponding values of the predictand's CS1 from the *reference* configuration. The median of these distributions is highlighted with a thick line. **c**, **d** Same as **b** but for CS2,3

circulation patterns related to the wind variability. We have analysed the sensitivity of this methodology to changes in five factors on the model configuration: number of retained EOF/CCA modes, chosen predictor field(s), extension of predictors' spatial domain, robustness of the method to data overfitting, and source of predictor variables. We have also evaluated the performance of the surface wind via this methodology in comparison with the direct model output of the different predictor sources (global reanalyses). The study has been undertaken with an observational network of 95 land sites, on a monthly time scale, during an extended wintertime season (NDJFM months), and for the 1980–2010 period. The results during the calibration period have helped us to extrapolate the analysis to the whole length of the observational dataset 1953–2010 and allowed a centennial assessment (1850–2010) of the wind field over this region on the basis of available large-scale predictor datasets and 20th century reanalysis products.

The variability over this region can be explained, to a large extend (59.3% for predictand, 55.3% for predictor), in terms of changes on three large-to-local scale atmospheric circulation modes. Due to the location of our region of interest these covariability modes are primarily related to AO/NAO patterns with very strong connections. Some modes, however, also show a weaker relationship with EA and EA-WR patterns, more influential over the Eastern North Atlantic. To a lesser extent PNA pattern, more relevant over the continent and the Pacific side, has also an effect over the area. The first mode explains a markedly superior fraction of variance (25–30%) than the rest ($\leq$ 20%). These modes of circulation can also be related, to certain extent, with months of extreme wind situations, establishing a partial relationship between monthly wind maxima and average monthly series.

The SD methodology used in this work has proven to be statistically robust via validation. Notwithstanding, the methodology is not free from uncertainties. An assessment on the methodological uncertainty has shown that the uncertainty on the wind field SD estimates depends to a large extent on the number of coupled circulation modes that are taken into account, but is for the most part unaffected by the choice of large-scale information source. The uncertainty is proportional to the variability of the sites. Among the five different parameters taken in account the number of EOF/CCA patterns is the most relevant one over the region, specially for meridional winds. Conversely, the large scale information provided by the global reanalyses is basically the same despite their widely varying assimilated data and their differences among the variety of models and methods.

Given an adequate choice of parameters the SD estimations are able to provide more realistic variances (standard deviation ratios between 0.6 and 1.0) than the reanalysis direct wind outputs (ratios between 0.5 and 3), but they show lower correlation values (0.6–0.9, significant at $p < 0.05$ for SD estimations against 0.7–0.97 for reanalyses, also significant). While the SD estimations are mostly insensitive to the reanalysis used, the reanalysis winds show notable differences in terms of their reproduced variance. These differences are not trivial to anticipate as they cannot be easily attributed to reanalysis characteristics such as horizontal resolution or amount of assimilated data, among others. The reanalyses that show the best results are JRA55 and JRA55C, followed by MERRA and Cera-20C. Their performances tend to cluster regionally. In contrast, the reanalysis with the comparatively poorest performances are DOE-R2, followed by 20CRv2c and Era-40. CFSR, one of the newest reanalysis and with the highest grid resolution performs comparatively worse than NCAR-R1, the first of the reanalysis products. Both the SD estimations and reanalysis products offer a more realistic characterization of zonal wind: the zonal flows that characterise the circulation over this region are largely dependent on the large-to-local scale relationships.

A reconstruction of the wind field over the last 160 years has been conducted, using all available reanalyses and two additional SLP gridded datasets as large scale information. A sensitivity analysis similar to that conducted for the calibration period has shown that there is a considerable agreement among the estimations obtained from the different sources until the middle of the 20th century, also coherent with the observed wind during the overlapping period. Some discrepancies are, however, observed for earlier periods. The reconstructions evidence variability at interannual as well as interdecadal timescales. There are no overall long-term trends in the multidecadal context. The discrepancies in the estimations are attributable to systematic biases produced by the scarcity and quality of assimilated observational data in the 20CRv2c 20th reanalysis during the 1860s–1880s decades.

The SD methodology and wind reanalyses have proved to shed reasonable estimations of the regional and local wind variability at monthly resolution. The exercise on the model sensitivity and wind reconstructions offers valuable information that can be extended to other seasons and timescales. For instance, the analysis of the summertime season, characterized by the extratropical storms from tropical origin such as hurricanes, might pose an interesting challenge.

Acknowledgements EELE was supported by the Agreement of Cooperation 4164281 between the UCM and St. Francis Xavier University, and the ILMODELS (CGL2014-59644-R) and NEWA (PCIN-2014-017-C07-06) projects of the MINECO (Spain). Funding for 4164281 was provided by the Natural Sciences and Engineering Research Council of Canada (NSERC DG 140576948), the Canada Research Chairs Program (CRC 230687), and the Atlantic Innovation Fund (AIF-ACOA). HB holds a Canada Research Chair in Climate Dynamics. EGB and JFGR held James Chair visiting Professorships (2017) at StFX University. JN, EGB and JFGR were supported by NEWA (PCIN-2014-017-C07-03, PCIN-2014-017-C07-06) and

NEWA2 (PCIN-2016-176, PCIN-2016-009) projects of the MINECO (Spain). This research has been conducted under the Joint Research Unit between UCM and CIEMAT, by the Colaboration Agreement 7158/2016. pecial thanks to Douglas Schuster for information regarding the assimilation of surface wind land observations in NCAR-R1, DOE-R2 and CFSR reanalyses.

Note: a version of the observational data used in this study will be made to the public. Likewise, the wind climatologies showed in the manuscript will also be available. Potential users interested in having the data are invited to contact the corresponding author.

References

Allan R, Ansell T (2006) A new globally complete monthly historical gridded mean sea level pressure dataset (hadslp2): 1850–2004. J Clim 19(22):5816–5842

Athanasiadis PJ, Wallace JM, Wettstein JJ (2010) Patterns of wintertime jet stream variability and their relation to the storm tracks. J Atmos Sci 67(5):1361–1381. https://doi.org/10.1175/2009JAS3270.1

Barnett T, Preisendorfer R (1987) Origins and levels of monthly and seasonal forecast skill for united states surface air temperatures determined by canonical correlation analysis. Mon Weather Rev 115:1825–1850

Barnston AG, Livezey RE (1987) Classification, seasonality and persistence of low-frequency atmospheric circulation patterns. Mon Weather Rev 115(6):1083–1126

Befort DJ, Wild S, Kruschke T, Ulbrich U, Leckebusch GC (2016) Different long-term trends of extra-tropical cyclones and windstorms in ERA-20C and NOAA-20CR reanalyses. Atmos Sci Lett 17(11):586–595. https://doi.org/10.1002/asl.694

Benestad RE (2001) A comparison between two empirical downscaling strategies. Int J Climatol 21:1645–1668. https://doi.org/10.1002/joc.703

Bollmeyer C, Keller JD, Ohlwein C, Wahl S, Crewell S, Friederichs P, Hense A, Keune J, Kneifel S, Pscheidt I, Redl S, Steinke S (2015) Towards a high-resolution regional reanalysis for the european CORDEX domain. Q J R Meteorol Soc 141(686):1–15. https://doi.org/10.1002/qj.2486

Bonsal BR, Shabbar A (2008) Impacts of large-scale circulation variability on low streamflows over Canada: a review. Can Water Resour J/Revue canadienne des ressources hydriques 33(2):137–154. https://doi.org/10.4296/cwrj3302137

Booth JF, Rieder HE, Lee DE, Kushnir Y (2015) The path of extratropical cyclones associated with wintertime high-wind events in the northeastern United states. J Appl Meteorol Climatol 54:1871–1885. https://doi.org/10.1175/JAMC-D-14-0320.1

Brinckmann S, Krähenmann S, Bissolli P (2016) High-resolution daily gridded data sets of air temperature and wind speed for Europe. Earth Syst Sci Data 8(2):491–516. https://doi.org/10.5194/essd-8-491-2016. https://www.earth-syst-sci-data.net/8/491/2016/. Accessed 9 Oct 2017

Cane MA (1986) El Niño. Annu Rev Earth Planet Sci 14:43–70. https://doi.org/10.1017/CBO9781107415324.004

Cattell RB (1966) The scree test for the number of factors. Multivar Behav Res 1(2):245–276

Cavazos T, Hewitson BC (2005) Performance of NCEP NCAR reanalysis variables in statistical downscaling of daily precipitation. Clim Res 28(MARCH):95–107

Cheng CS (2014) Evidence from the historical record to support projection of future wind regimes: an application to Canada. Atmos Ocean 52(3):232–241. https://doi.org/10.1080/07055900.2014.902803

Cheng CS, Lopes E, Fu C, Huang Z (2014) Possible impacts of climate change on wind gusts under downscaled future climate conditions: updated for Canada. J Clim 27(3):1255–1270. https://doi.org/10.1175/JCLI-D-13-00020.1

CISL RDA (1979) Data Support Section, Computational and Information Systems Laboratory, National Center for Atmospheric Research, University Corporation for Atmospheric Research and National Weather Service, NOAA, U.S. Department of Commerce and Dept. of Earth, Atmospheric, and Planetary Sciences, Massachusetts Institute of Technology and Met Office, Ministry of Defence, United Kingdom and National Climatic Data Center, NESDIS, NOAA, U.S. Department of Commerce and Naval Research Laboratory, Monterey, U.S. Navy, U. S. Department of Defense and National Centers for Environmental Prediction, National Weather Service, NOAA, U.S. Department of Commerce. Daily Northern Hemisphere Sea Level Pressure Grids, continuing from 1899. http://rda.ucar.edu/datasets/ds010.0/. Accessed 6 May 2015

CISL RDA (2007) Japan Meteorological Agency/Japan, and Central Research Institute of Electric Power Industry/Japan. Japanese 25-year Reanalysis Project. http://rda.ucar.edu/datasets/ds625.0/. Accessed 22 May 2015

CISL RDA (2008) Japan Meteorological Agency/Japan, and Central Research Institute of Electric Power Industry/Japan. Japanese 25-year Reanalysis Project, Monthly Means. http://rda.ucar.edu/datasets/ds625.1/. Accessed 24 May 2015

CISL RDA (2010) Saha, S., et al.: NCEP Climate Forecast System Reanalysis (CFSR) Monthly Products, January 1979 to December 2010. https://doi.org/10.5065/D6DN438J, http://rda.ucar.edu/datasets/ds093.2/. Accessed 25 May 2015

CISL RDA (2013) Japan Meteorological Agency/Japan. JRA-55: Japanese 55-year Reanalysis, Monthly Means and Variances. https://rda.ucar.edu/datasets/ds628.1/. Accessed 23 April 2015

CISL RDA (2015a) Gilbert P. Compo, et al.: NOAA/CIRES Twentieth Century Global Reanalysis Version 2c. Updated yearly. https://doi.org/10.5065/D6N877TW, http://rda.ucar.edu/datasets/ds131.2/. Accessed 4 June 2015

CISL RDA (2015b) Meteorological Research Institute/Japan Meteorological Agency/Japan. JRA-55C: Monthly Means and Variances. https://rda.ucar.edu/datasets/ds628.3/. Accessed 10 May 2017

Cleugh H, Miller J, Böhm M (1998) Direct mechanical effects of wind on crops. Agrofor Syst 41(1):85–112

Compo GP, Whitaker JS, Sardeshmukh PD, Matsui N, Allan RJ, Yin X, Gleason BE, Vose RS, Rutledge G, Bessemoulin P, BroNnimann S, Brunet M, Crouthamel RI, Grant AN, Groisman PY, Jones PD, Kruk MC, Kruger AC, Marshall GJ, Maugeri M, Mok HY, Nordli O, Ross TF, Trigo RM, Wang XL, Woodruff SD, Worley SJ (2011) The twentieth century reanalysis project. Q J R Meteorol Soc 137(654):1–28. https://doi.org/10.1002/qj.776

Conrad CT (2009) Severe and hazardous weather in canada: the geography of extreme events. Oxford University Press, Oxford

Cram T, Compo GP, Yin X, Allan RJ, McColl C, Vose RS, Whitaker JS, Matsui N, Ashcroft L, Auchmann R, Bessemoulin P, Brandsma T, Brohan P, Brunet M, Comeaux J, Crouthamel R, Gleason BE, Groisman PY, Hersbach H, Jones PD, Jónsson T, Jourdain S, Kelly G, Knapp KR, Kruger A, Kubota H, Lentini G, Lorrey A, Lott N, Lubker SJ, Luterbacher J, Marshall GJ, Maugeri M, Mock CJ, Mok HY, Oy N, Rodwell MJ, Ross TF, Schuster D, Srnec L, Valente MA, Vizi Z, Wang XL, Westcott N, Woollen JS, Worley SJ (2015) The international surface pressure databank version 2. Geosci Data J 2(1):31–46. https://doi.org/10.1002/gdj3.25

Culver AMR, Monahan AH (2013) The statistical predictability of surface winds over western and central Canada. J Clim 26(21):8305–8322. https://doi.org/10.1175/JCLI-D-12-00425.1

Curry CL, van der Kamp D, Monahan AH (2012) Statistical downscaling of historical monthly mean winds over a coastal region of complex terrain. I. Predicting wind components. Clim Dyn 38:1281–1299. https://doi.org/10.1007/s00382-011-1175-1

Darby LS (2005) Cluster analysis of surface winds in Houston, Texas, and the impact of wind patterns on ozone. J Appl Meteorol 44(12):1788–1806

Dee D, Uppala S, Simmons A, Berrisford P, Poli P, Kobayashi S, Andrae U, Balmaseda M, Balsamo G, Bauer P (2011) The era-interim reanalysis: configuration and performance of the data assimilation system. Q J R Meteorol Soc 137(656):553–597. https://doi.org/10.1002/qj.828

Ebita A, Kobayashi S, Ota Y, Moriya M, Kumabe R, Onogi K, Harada Y, Yasui S, Miyaoka K, Takahashi K, Kamahori H, Kobayashi C, Endo H, Soma M, Oikawa Y, Ishimizu T (2011) The Japanese 55-year Reanalysis jra-55: an interim report. Sola 7:149–152. https://doi.org/10.2151/sola.2011-038

Farquhar G, Roderick M (2005) Worldwide changes in evaporative demand. Water Environ 12:81–99

Ferguson CR, Villarini G (2014) An evaluation of the statistical homogeneity of the twentieth century reanalysis. Clim Dyn 42(11–12):2841–2866. https://doi.org/10.1007/s00382-013-1996-1

Fowler H, Blenkinsop S, Tebaldi C (2007) Linking climate change modelling to impacts studies: recent advances in downscaling techniques for hydrological modelling. Int J Climatol 27(12):1547–1578. https://doi.org/10.1002/joc.1556

Frias MD, Zorita E, Fernandez J, Rodriguez-Puebla C (2006) Testing statistical downscaling methods in simulated climates. Geophys Res Lett 33(19):1–5. https://doi.org/10.1029/2006GL027453

Fujiwara M, Wright JS, Manney GL, Gray LJ, Anstey J, Birner T, Davis S, Gerber EP, Lynn Harvey V, Hegglin MI, Homeyer CR, Knox JA, Krüger K, Lambert A, Long CS, Martineau P, Molod A, Monge-Sanz BM, Santee ML, Tegtmeier S, Chabrillat S, Tan DG, Jackson DR, Polavarapu S, Compo GP, Dragani R, Ebisuzaki W, Harada Y, Kobayashi C, McCarty W, Onogi K, Pawson S, Simmons A, Wargan K, Whitaker JS, Zou CZ (2017) Introduction to the SPARC Reanalysis Intercomparison Project (S-RIP) and overview of the reanalysis systems. Atmos Chem Phys 17(2):1417–1452. https://doi.org/10.5194/acp-17-1417-2017

García-Bustamante E, González-Rouco JF, Pa J, Navarro J, Montávez JP (2008) The influence of the Weibull assumption in monthly wind energy estimation. Wind Energy 11(5):483–502. https://doi.org/10.1002/we.270

García-Bustamante E, González-Rouco J, Jiménez P, Navarro J, Montávez J (2009) A comparison of methodologies for monthly wind energy estimation. Wind Energy 12(7):640–659. https://doi.org/10.1002/we.315

García-Bustamante E, González-Rouco JF, Navarro J, Xoplaki E, Pa J, Montávez JP (2011) North Atlantic atmospheric circulation and surface wind in the Northeast of the Iberian Peninsula: uncertainty and long term downscaled variability. Clim Dyn 38(1–2):141–160. https://doi.org/10.1007/s00382-010-0969-x

García-Bustamante E, González-Rouco JF, Navarro J, Xoplaki E, Luterbacher J, Jiménez PA, Montávez JP, Hidalgo A, Lucio-Eceiza EE (2012) Relationship between wind power production and North Atlantic atmospheric circulation over the northeastern Iberian Peninsula. Clim Dyn 40:935–949. https://doi.org/10.1007/s00382-012-1451-8

González-Rouco JF, Heyen H, Zorita E, Valero F (2000) Agreement between observed rainfall trends and climate change simulations in the Southwest of Europe. J Clim 13(17):3057–3065. https://doi.org/10.1175/1520-0442(2000)013<3057:ABORTA>2.0.CO;2

Grise KM, Son SW, Gyakum JR (2013) Intraseasonal and interannual variability in North American storm tracks and its relationship to equatorial pacific variability. Mon Weather Rev 141(10):3610–3625. https://doi.org/10.1175/MWR-D-12-00322.1

Gulev SK, Zolina O, Grigoriev S (2001) Extratropical cyclone variability in the Northern Hemisphere winter from the NCEP/NCAR reanalysis data. Clim Dyn 17(10):795–809. https://doi.org/10.1007/s003820000145

Hart RE, Evans JL (2001) A climatology of the extratropical transition of Atlantic tropical cyclones. J Clim 14(4):546–564. https://doi.org/10.1175/1520-0442(2001)014<0546:ACOTET>2.0.CO;2

Hayden BP (1981) Secular variation in atlantic coast extratropical cyclones. Mon Weather Rev 109(January):159–167

Hersbach H, Poli P, Dee D (2015) The observation feedback archive for the ICOADS and ISPD data sets (ERA-20C). Report Series 18. Tech. rep., ECMWF

Hertig E, Jacobeit J (2014) Considering observed and future non-stationarities in statistical downscaling of Mediterranean precipitation. Theor Appl Climatol 122:667–683. https://doi.org/10.1007/s00704-014-1314-9

Hertig E, Paxian A, Vogt G, Seubert S, Paeth H, Jacobeit J (2012) Statistical and dynamical downscaling assessments of precipitation extremes in the Mediterranean area. Meteorologische Zeitschrift 21(1):61–77. https://doi.org/10.1127/0941-2948/2012/0271

Hughes L, Chaudhry N (2011) The challenge of meeting Canadas greenhouse gas reduction targets. Energy Policy 39(3):1352–1362. https://doi.org/10.1016/j.enpol.2010.12.007

Hurrell JW (1995) Decadal trends in the North Atlantic oscillation: regional temperatures and precipitation. Science (New York, NY) 269(5224):676–9. https://doi.org/10.1126/science.269.5224.676

Huth R (2002) Statistical downscaling of daily temperature in central Europe. J Clim 15(13):1731–1742. https://doi.org/10.1175/1520-0442(2002)015<1731:SDODTI>2.0.CO;2

Isard S, Angel JR, VanDyke GT (2000) Zones of origin for Great Lakes Cyclones in North America, 1899–1996. Mon Weather Rev 28(2):474. https://doi.org/10.1175/1520-0493(2000)128<0474:ZOOFGL>2.0.CO;2

Jakob Themeßl M, Gobiet A, Leuprecht A (2011) Empirical-statistical downscaling and error correction of daily precipitation from regional climate models. Int J Climatol 31(10):1530–1544. https://doi.org/10.1002/joc.2168

Jiménez P, González-Rouco J, García-Bustamante E, Navarro J, Montávez J, de Arellano J, Dudhia J, Muñoz-Roldan A (2010) Surface wind regionalization over complex terrain: evaluation and analysis of a high-resolution wrf simulation. J Appl Meteorol Climatol 49(2):268–287. https://doi.org/10.1175/2009JAMC2175.1

Jiménez PA, González-Rouco JF, Montávez JP, García-Bustamante E (2008) Climatology of wind patterns in the northeast of the Iberian Peninsula. Int J Climatol 29:501–525. https://doi.org/10.1002/joc

Kaas E, Li TS, Schmith T (1996) Statistical hindcast of wind climatology in the north atlantic and northwestern european region. Clim Res 7(2):97–110

Kalnay E, Kanamitsu M, Kistler R, Collins W, Deaven D, Gandin L, Iredell M, Saha S, White G, Woollen J, Zhu Y, Chelliah M, Ebisuzaki W, Higgins W, Janowiak J, Mo KC, Ropelewski C, Wang J, Leetmaa A, Reynolds R, Jenne R, Joseph D (1996) The NCEP/NCAR 40-year reanalysis project. Bull Am Meteorol Soc 77(3):437–471. https://doi.org/10.1175/1520-0477(1996)077<0437:TNYRP>2.0.CO;2

van der Kamp D, Curry CL, Monahan AH (2012) Statistical downscaling of historical monthly mean winds over a coastal region of complex terrain. II. Predicting wind components. Clim Dyn 38:1301–1311. https://doi.org/10.1007/s00382-011-1175-1

Kanamitsu M, Ebisuzaki W, Woollen J, Yang SK, Hnilo JJ, Fiorino M, Potter GL (2002) NCEP-DOE AMIP-II reanalysis (R-2).

Bull Am Meteorol Soc 83(11):1631–1643+1559. https://doi.org/10.1175/BAMS-83-11-1631

Khanduri A, Morrow G (2003) Vulnerability of buildings to windstorms and insurance loss estimation. J Wind Eng Ind Aerodyn 91(4):455–467

Klink K (1999a) Climatological mean and interannual variance of United States surface wind speed, direction and velocity. Int J Climatol 19(5):471–488. https://doi.org/10.1002/(SICI)1097-0088(199904)19:5<471::AID-JOC367>3.0.CO;2-X

Klink K (1999b) Trends in mean monthly maximum and minimum surface wind speeds in the coterminous United States, 1961 to 1990. Clim Res 13(3):193–205. https://doi.org/10.3354/cr013193

Kobayashi C, Endo H, Ota Y, Kobayashi S, Onoda H, Harada Y, Onogi K, Kamahori H (2014) Preliminary results of the jra-55c, an atmospheric reanalysis assimilating conventional observations only. Sola 10:78–82. https://doi.org/10.2151/sola.2014-016

Laloyaux P, Balmaseda M, Dee D, Mogensen K, Janssen P (2016) A coupled data assimilation system for climate reanalysis. Q J R Meteorol Soc 142(694):65–78. https://doi.org/10.1002/qj.2629

Lindsay R, Wensnahan M, Schweiger A, Zhang J (2014) Evaluation of seven different atmospheric reanalysis products in the Arctic. J Clim 27(7):2588–2606. https://doi.org/10.1175/JCLI-D-13-00014.1

Lucio-Eceiza EE, González-Rouco JF, Navarro J, Beltrami H (2018a) Quality Control of surface wind observations in North Eastern North America. Part I: Data management issues. J Atmos Ocean Technol 35:163–182. https://doi.org/10.1175/JTECH-D-16-0204.1

Lucio-Eceiza EE, González-Rouco JF, Navarro J, Beltrami H, Conte J (2018b) Quality Control of surface wind observations in North Eastern North America. Part II: Measurement errors. J Atmos Ocean Technol 35:183–205. https://doi.org/10.1175/JTECH-D-16-0205.1

Mailier PJ, Stephenson DB, CaT F, Hodges KI (2006) Serial clustering of extratropical cyclones. Mon Weather Rev 134(8):2224–2240. https://doi.org/10.1175/MWR3160.1

Mantua NJ, Hare SR, Zhang Y, Wallace JM, Francis RC (1997) A Pacific interdecadal climate oscillation with impacts on salmon production. Bull Am Meteorol Soc 78(January):1069–1079. https://doi.org/10.1175/1520-0477(1997)078h1069:APICOWi2.0.CO;2

Martinez Y, Yu W, Lin H (2013) A new statistical-dynamical downscaling procedure based on eof analysis for regional time series generation. J Appl Meteorol Climatol 52(4):935–952. https://doi.org/10.1175/JAMC-D-11-065.1

McVicar TR, Roderick ML, Donohue RJ, Li LT, Van Niel TG, Thomas A, Grieser J, Jhajharia D, Himri Y, Mahowald NM, Mescherskaya AV, Kruger AC, Rehman S, Dinpashoh Y (2012) Global review and synthesis of trends in observed terrestrial near-surface wind speeds: implications for evaporation. J Hydrol 416–417:182–205. https://doi.org/10.1016/j.jhydrol.2011.10.024

Mesinger F, DiMego G, Kalnay E, Mitchell K, Shafran PC, Ebisuzaki W, Jović D, Woollen J, Rogers E, Berbery EH, Ek MB, Fan Y, Grumbine R, Higgins W, Li H, Lin Y, Manikin G, Parrish D, Shi W (2006) North American regional reanalysis. Bull Am Meteorol Soc 87(3):343–360. https://doi.org/10.1175/BAMS-87-3-343

Najac J, Boé J, Terray L (2009) A multi-model ensemble approach for assessment of climate change impact on surface winds in France. Clim Dyn 32(5):615–634. https://doi.org/10.1007/s00382-008-0440-4

National Center for Atmospheric Research (2016) The Climate Data Guide: Hurrell North Atlantic Oscillation (NAO) Index (PC-based)

North GR, Moeng FJ, Bell TL, Cahalan RF, Moeng FJ, Bell TL, Cahalan RF (1982) The latitude dependence of the variance of zonally averaged quantities. Mon Weather Rev 110(5):319–326. https://doi.org/10.1175/1520-0493(1982)110<0319:TLDOTV>2.0.CO;2

Ogi M, Tachibana Y, Yamazaki K (2003) Impact of the wintertime north atlantic oscillation (nao) on the summertime atmospheric circulation. Geophys Res Lett 22:22. https://doi.org/10.1029/2003GL017280

Onogi K, Tsutsi J, Koide H, Sakamoto M, Kobayashi S, Hatsushika H, Matsumoto T, Yamazaki N, Kamahori H, Takahashi K, Kadokura S, Wada K, Kato K, Oyama R, Ose T, Mannoji N, Taira R (2007) The JRA-25 reanalysis. J Meteorol Soc Jpn 85(3):369–432. https://doi.org/10.2151/jmsj.85.369

Plante M, Son SW, Atallah E, Gyakum J, Grise K (2014) Extratropical cyclone climatology across eastern Canada. Int J Climatol 35(10):2759–2776. https://doi.org/10.1002/joc.4170

Poli P, Hersbach H, Dee DP, Berrisford P, Simmons AJ, Vitart F, Laloyaux P, Tan DGH, Peubey C, Thépaut JN, Trémolet Y, Hólm EV, Bonavita M, Isaksen L, Fisher M (2016) ERA-20C: An atmospheric reanalysis of the twentieth century. J Clim 29(11):4083–4097. https://doi.org/10.1175/JCLI-D-15-0556.1

Pryor SC, Barthelmie RJ (2014) Hybrid downscaling of wind climates over the eastern USA. Environ Res Lett 9(2):024013. https://doi.org/10.1088/1748-9326/9/2/024013

Pryor SC, Schoof JT, Barthelmie RJ (2005) Climate change impacts on wind speeds and wind energy density in Northern Europe: empirical downscaling of multiple AOGCMs. Clim Res 29(3):183–198. https://doi.org/10.3354/cr029183

Pryor SC, Schoof JT, Barthelmie RJ (2006) Winds of change?: Projections of near-surface winds under climate change scenarios. Geophys Res Lett 33(11):1–5. https://doi.org/10.1029/2006GL026000

Pryor SC, Barthelmie RJ, Young DT, Takle ES, Arritt RW, Flory D, Jr WJG, Nunes A, Roads J (2009) Wind speed trends over the contiguous United States. J Geophys Res 114:18. https://doi.org/10.1029/2008JD011416

Pryor SC, Barthelmie RJ, Schoof JT (2012) Past and future wind climates over the contiguous USA based on the North American Regional Climate Change Assessment Program model suite. J Geophys Res 117:1–17. https://doi.org/10.1029/2012JD017449

Rasmusson EM, Wallace JM (1983) Meterogical aspects of the El Niño. Science 222:1195–1202. https://doi.org/10.1126/science.222.4629.1195

REN21 (2017) Renewables 2017 global status report. (Paris: REN21 Secretariat). ISBN: 978-3-9818107-0-7. https://doi.org/10.1016/j.rser.2016.09.082

Richards W, Abuamer Y (2007) Atmospheric hazards: extreme wind gust climatology in Atlantic Canada 1955–2000. Tech. rep, Meteorological Service of Canada, Atlantic

Richman MB (1986) Rotation of principal components. J Climatol 6(3):293–335. https://doi.org/10.1002/joc.3370060305

Rienecker MM, Suarez MJ, Gelaro R, Todling R, Bacmeister J, Liu E, Bosilovich MG, Schubert SD, Takacs L, Kim GK, Bloom S, Chen J, Collins D, Conaty A, Da Silva A, Gu W, Joiner J, Koster RD, Lucchesi R, Molod A, Owens T, Pawson S, Pegion P, Redder CR, Reichle R, Robertson FR, Ruddick AG, Sienkiewicz M, Woollen J (2011) MERRA: NASA's modern-era retrospective analysis for research and applications. J Clim 24(14):3624–3648. https://doi.org/10.1175/JCLI-D-11-00015.1

Ropelewski CF, Jones PD (1987) An extension of the Tahiti Darwin Southern Oscillation Index. Mon Weather Rev 115:2161–2165. https://doi.org/10.1175/1520-0493(1987)115h2161:AEOTTSi2.0.CO;2

Saha S, Moorthi S, Pan HL, Wu X, Wang J, Nadiga S, Tripp P, Kistler R, Woollen J, Behringer D, Liu H, Stokes D, Grumbine R, Gayno G, Wang J, Hou YT, Chuang HY, Juang HMH, Sela J, Iredell M, Treadon R, Kleist D, Van Delst P, Keyser D, Derber J, Ek

M, Meng J, Wei H, Yang R, Lord S, Van Den Dool H, Kumar A, Wang W, Long C, Chelliah M, Xue Y, Huang B, Schemm JK, Ebisuzaki W, Lin R, Xie P, Chen M, Zhou S, Higgins W, Zou CZ, Liu Q, Chen Y, Han Y, Cucurull L, Reynolds RW, Rutledge G, Goldberg M (2010) The NCEP climate forecast system reanalysis. Bull Am Meteorol Soc 91(8):1015–1057. https://doi.org/10.1175/2010BAMS3001.1

Siegismund F, Schrum C (2001) Decadal changes in the wind forcing over the north sea. Clim Res 18:39–45. https://doi.org/10.3354/cr018039

Stewart R, Bachand D, Dunkley R, Giles A, Lawson B, Legal L, Miller S, Murphy B, Parker M, Paruk B (1995) Winter storms over canada. Atmos Ocean 33(2):223–247. https://doi.org/10.1080/07055900.1995.9649533

von Storch H, Zwiers FW (2003) Statistical analysis in climate research. Cambridge University Press, Cambridge

Storch H, Zorita E, Cubasch U (1993) Downscaling of global climate change estimates to regional scales: an application to Iberian rainfall in wintertime. J Clim 6:1161–1171. https://doi.org/10.1175/1520-0442(1993)006<1161:DOGCCE>2.0.CO;2

Taylor KE (2001) Summarizing multiple aspects of model performance in a single diagram. J Geophys Res 106(D7):7183–7192. https://doi.org/10.1029/2000JD900719

Taylor KE, Stouffer RJ, Meehl GA (2012) An overview of cmip5 and the experiment design. Bull Am Meteorol Soc 93(4):485–498. https://doi.org/10.1175/BAMS-D-11-00094.1

Thomas BC, Martin JE (2007) A synoptic climatology and composite analysis of the alberta clipper. Weather Forecast 22(2):315–333. https://doi.org/10.1175/WAF982.1

Thompson DWJ, Wallace JM (1998) The Arctic oscillation signature in the wintertime geopotential height and temperature fields. Geophys Res Lett 25(9):1297. https://doi.org/10.1029/98GL00950

Thompson DWJ, Wallace JM (2000a) Annular mode in the extratropical circulation. Part I : month-to-month variability. J Clim 13(1999):1000–1016. https://doi.org/10.1175/1520-0442(2000)013<1000:AMITEC>2.0.CO;2

Thompson DWJ, Wallace JM (2000b) Annular modes in the extratropical circulation. Part II: trends. J Clim 13(5):1018–1036. https://doi.org/10.1175/1520-0442(2000)013<1018:AMITEC>2.0.CO;2

Torralba V, Doblas-Reyes FJ, González-Reviriego N (2017) Uncertainty in recent near-surface wind speed trends: a global reanalysis intercomparisonparison. Environ Res Lett 12:10

Torrence C, Compo GP (1998) A practical guide to wavelet analysis. Bull Am Meteorol Anal 79(1):61–78. https://doi.org/10.1175/1520-0477(1998)079<0061:APGTWA>2.0.CO;2

Trenberth KE (1984) Signal versus noise in the southern oscillation. Mon Weather Rev 112:326–332. https://doi.org/10.1175/1520-0493(1984)112<0326:SVNITS>2.0.CO;2

Trenberth KE, Hurrell JW (1994) Decadal atmosphere-ocean variations in the Pacific. Clim Dyn 9(6):303–319. https://doi.org/10.1007/BF00204745

Tuller SE (2004) Measured wind speed trends on the west coast of Canada. Int J Climatol 24(11):1359–1374. https://doi.org/10.1002/joc.1073

Ulbrich U, Leckebusch GC, Pinto JG (2009) Extra-tropical cyclones in the present and future climate: a review. Theor Appl Climatol 96(1–2):117–131. https://doi.org/10.1007/s00704-008-0083-8

Uppala SM, Kallberg PW, Simmons AJ, Andrae U, Bechtold VDC, Fiorino M, Gibson JK, Haseler J, Hernandez A, Kelly GA, Li X, Onogi K, Saarinen S, Sokka N, Allan RP, Andersson E, Arpe K, Balmaseda MA, Beljaars ACM, Berg LVD, Bidlot J, Bormann N, Caires S, Chevallier F, Dethof A, Dragosavac M, Fisher M, Fuentes M, Hagemann S, Hólm E, Hoskins BJ, Isaksen L, Janssen PAEM, Jenne R, Mcnally AP, Mahfouf JF, Morcrette JJ, Rayner NA, Saunders RW, Simon P, Sterl A, Trenberth KE, Untch A, Vasiljevic D, Viterbo P, Woollen J (2005) The ERA-40 re-analysis. Q J R Meteorol Soc 131(612):2961–3012. https://doi.org/10.1256/qj.04.176

Wallbrink H, Koek F, Brandsma T (2009) The US Maury collection metadata 1796–1861. Koninklijk Nederlands Meteorologisch Instituut

Wan H, Wang XL, Swail VR (2010) Homogenization and trend analysis of Canadian near-surface wind speeds. J Clim 23(5):1209. https://doi.org/10.1175/2009JCLI3200.1

Wang XL, Wan H, Swail VR (2006) Observed changes in cyclone activity in Canada and their relationships to major circulation regimes. J Clim 19:896–915. https://doi.org/10.1175/JCLI3664.1

Wang XL, Feng Y, Compo GP, Swail VR, Zwiers FW, Allan RJ, Sardeshmukh PD (2013) Trends and low frequency variability of extra-tropical cyclone activity in the ensemble of twentieth century reanalysis. Clim Dyn 40(11–12):2775–2800. https://doi.org/10.1007/s00382-012-1450-9

Wang YH, Magnusdottir G, Stern H, Tian X, Yu Y (2012) Decadal variability of the NAO: introducing an augmented NAO index. Geophys Res Lett 39(21):1–5. https://doi.org/10.1029/2012GL053413

Wilby RL, Charles SP, Zorita E, Timbal B, Whetton P, Mearns LO (2004) Guidelines for use of climate scenarios developed from statistical downscaling methods. Tech. Rep. August, http://www.narccap.ucar.edu/doc/tgica-guidance-2004.pdf. Accessed 28 Dec 2016

Wiser R, Bolinger M (2016) 2015 Wind technologies market report. Tech. Rep. August, U.S. Department of Energy

WMO (2011) Guide to climatological practices WMO-No. 100, 2011th edn. 100, World Meteorological Organization (WMO), Geneva, Switzerland, WMO-No. 100

Wójcik R (2015) Reliability of CMIP5 GCM simulations in reproducing atmospheric circulation over Europe and the North Atlantic: a statistical downscaling perspective. Int J Climatol 35(5):714–732. https://doi.org/10.1002/joc.4015

Woodruff SD, Diaz HF, Worley SJ, Reynolds RW, Lubker SJ (2005) Early ship observational data and icoads. Clim Change 73(1):169–194. https://doi.org/10.1007/s10584-005-3456-3

Wu J, Zha J, Zhao D (2016) Evaluating the effects of land use and cover change on the decrease of surface wind speed over China in recent 30 years using a statistical downscaling method. Clim Dyn 48:1–19. https://doi.org/10.1007/s00382-015-2616-z

Xoplaki E, González-Rouco JF, Luterbacher J, Wanner H (2003) Mediterranean summer air temperature variability and its connection to the large-scale atmospheric circulation and SSTs. Clim Dyn 20(7–8):723–739. https://doi.org/10.1007/s00382-003-0304-x

Xoplaki E, González-Rouco JF, Luterbacher J, Wanner H (2004) Wet season Mediterranean precipitation variability: influence of large-scale dynamics and trends. Clim Dyn 23(1):63–78. https://doi.org/10.1007/s00382-004-0422-0

Zhang Y, Wallace JM, Battisti DS (1997) ENSO-like interdecadal variability: 1900–93. J Clim 10(5):1004–1020. https://doi.org/10.1175/1520-0442(1997)010<1004:ELIV>2.0.CO;2

Zha J, Wu J, Zhao D, Yang Q (2017) Changes of the probabilities in different ranges of near-surface wind speed in China during the period for 1970–2011. J Wind Eng Ind Aerodyn 169:156–167. https://doi.org/10.1016/j.jweia.2017.07.019

Zielinski G (2002) A classification scheme for winter storms in the Eastern and Central United States with an emphasis on Nor'easters. Bull Am Meteorol Soc 83(1):37–51. https://doi.org/10.1175/1520-0477(2002)083<0037:ACSFWS>2.3.CO;2

Zorita E, von Storch H (1999) The analog method as a simple statistical downscaling technique: comparison with more complicated methods. J Clim 12(8 PART 2):2474–2489. https://doi.org/10.1175/1520-0442(1999)012<2474:TAMAAS>2.0.CO;2